

**University POLITEHNICA of Bucharest**

**Faculty of Applied Chemistry and Materials Science**

**Department of Organic Chemistry "Costin D. NENITESCU"**



## **Ph.D. THESIS SUMMARY**

**Thesis Supervisor:**  
**Prof. dr. eng. Raluca Stan**

**Ph.D. Candidate:**  
**Alina Moroşan**

**Bucharest**  
**2020**

**University POLITEHNICA of Bucharest**

**Faculty of Applied Chemistry and Materials Science**

**Department of Organic Chemistry "Costin D. NENITESCU"**



# **Magnetic nanostructured systems with applications in peptide synthesis and electronics**

**Thesis Supervisor:**  
**Prof. dr. eng. Raluca Stan**

**Ph.D. Candidate:**  
**Alina Moroşan**

**Bucharest**  
**2020**

## CONTENTS

<b>LIST OF ABBREVIATIONS</b> .....	<b>9</b>
<b>INTRODUCTION</b> .....	<b>13</b>
<b>I. CRITICAL STUDY OF LITERATURE DATA</b> .....	<b>15</b>
<b>CHAPTER 1. PEPTIDE SYNTHESIS</b> .....	<b>16</b>
1.1. Peptide synthesis. General notions. ....	16
1.2. Chemical peptide synthesis: Brief history. ....	22
1.3. Solid phase peptide synthesis (SPPS).....	24
1.3.1. Groups used to protect amino acid N-terminal peptide synthesis on solid support .....	25
1.3.2. Monitoring the coupling and deprotection stages .....	29
1.3.3. Selection of the resin used as a solid support and swelling properties.....	31
1.3.4. Linkers used in SPPS .....	33
1.3.5. Activation of the carboxyl group of amino acids.....	35
1.3.6. Specific particularities in SPPS .....	36
1.3.6.1. Racemization .....	36
1.3.6.2. Aspartimide formation.....	38
1.3.6.3. Peptide aggregation.....	39
1.4. Modern strategies for approaching solid phase peptide synthesis .....	40
1.4.1. Microwave-assisted SPPS (MW-SPPS) and SPPS using ultrasonic agitation... 40	
1.4.2. Green chemistry approach in SPPS.....	40
1.4.3. Nanocomposite materials in SPPS .....	41
1.5. Purification and characterization of synthesized peptides .....	44
<b>CHAPTER 2. MAGNETIC NANOPARTICLES BASED ON IRON</b> .....	<b>45</b>
2.1. Magnetic nanoparticles based on iron oxide. General notions .....	45
2.1.1. Magnetic properties of nanoparticles .....	46
2.2. Core-shell magnetic nanoparticles with organic shell .....	48
2.2.1. Methods for the synthesis of magnetic nanoparticles .....	49
2.2.1.1. Co-precipitation method.....	49
2.2.1.2. Microemulsion method.....	50
2.2.1.3. Sol-gel method .....	51
2.2.1.4. Thermal decomposition method of precursors .....	51
2.2.1.5. Hydrothermal method.....	52
2.2.1.6. Electrochemical method .....	53
2.2.1.7. Polyol method.....	54
2.2.1.8. Biomineralization .....	55
2.2.2. Surface modification of magnetic nanoparticles Fe <sub>3</sub> O <sub>4</sub> .....	56
2.2.2.1. Silica coating by sol-gel method .....	57
2.3. Applications of magnetic nanoparticles.....	59
2.3.1. Nuclear magnetic resonance imaging.....	62

2.3.2. Magnetic hyperthermia.....	63
2.3.3. Targeted delivery of drugs .....	63
2.3.4. Bioseparation.....	64
2.3.5. Detection of bacteria, viruses and proteins .....	64
2.3.6. Solid support in solid phase peptide synthesis .....	64
2.3.7. Applications in electronics .....	65
2.3.8. Environmental applications.....	65
2.3.9. Nano-organic catalysts .....	65
2.3.10. Industrial applications .....	66
<b>II. ORIGINAL CONTRIBUTIONS .....</b>	<b>67</b>
<b>CHAPTER 3. MATERIALS AND METHODS.....</b>	<b>68</b>
3.1. Materials used for obtaining magnetic nanostructured systems and in solid phase peptide synthesis.....	68
3.1.1. Materials used for the synthesis of core-shell magnetic nanoparticles/nanoparticles with functionalized silica shell and the synthesis of linker systems .....	68
3.1.2. Materials used for the solid phase peptide synthesis.....	68
3.1.3. Solvents .....	69
3.2. Methods of synthesis and techniques for the characterization of core-shell magnetic nanoparticles, nanoparticles with functionalized silica shell, linker systems, and peptide sequences synthesized .....	70
3.2.1. Methods of synthesis of nanostructured systems .....	70
<i>Synthesis of <b>Fe<sub>3</sub>O<sub>4</sub>-PABA</b> core-shell magnetic nanoparticles .....</i>	<i>70</i>
<i>Synthesis of <b>Fe<sub>3</sub>O<sub>4</sub>-PABA-SiO<sub>2</sub></b> magnetic nanoparticles with silica secondary shell</i>	<i>70</i>
a) Synthesis of <b>Fe<sub>3</sub>O<sub>4</sub>-PABA-SiO<sub>2</sub>-1</b> magnetic nanoparticles with silica secondary shell.....	70
b) Synthesis of <b>Fe<sub>3</sub>O<sub>4</sub>-PABA-SiO<sub>2</sub>-2</b> magnetic nanoparticles with silica secondary shell.....	71
c) Synthesis of <b>Fe<sub>3</sub>O<sub>4</sub>-PABA-SiO<sub>2</sub>-3</b> and <b>Fe<sub>3</sub>O<sub>4</sub>-PABA-SiO<sub>2</sub>-4</b> magnetic nanoparticles with silica secondary shell .....	71
<i>Synthesis of nanostructured systems used as a solid support in peptide synthesis .....</i>	<i>72</i>
a) Synthesis of <b>Fe<sub>3</sub>O<sub>4</sub>-PABA-GA-PPD</b> nanostructured system.....	72
b) Synthesis of <b>Fe<sub>3</sub>O<sub>4</sub>-PABA-SiO<sub>2</sub>-APS-HMBA</b> nanostructured system .....	72
c) Synthesis of <b>Fe<sub>3</sub>O<sub>4</sub>-PABA-SiO<sub>2</sub>-SiL-OH</b> nanostructured system .....	73
d) Synthesis of <b>Fe<sub>3</sub>O<sub>4</sub>-PABA-SiO<sub>2</sub>-SiL-OH<sub>mw</sub></b> nanostructured system.....	74
<i>Fabrication of transistor based on <b>Fe<sub>3</sub>O<sub>4</sub>-PABA</b> magnetic nanoparticles .....</i>	<i>74</i>
<i>Synthesis of <b>Fe<sub>3</sub>O<sub>4</sub>-PABA-SiO<sub>2</sub></b> nanofilm doped with <b>DPPH</b> radical.....</i>	<i>75</i>
3.2.2. Synthesis of peptides on magnetic nanostructured support.....	75
a) Synthesis of <b>Lys-Ala-Gly</b> .....	75
b) Synthesis of <b>Val-Ile- Lys</b> .....	76
c) Synthesis of <b>Gly-Ala-Phe</b> .....	78

d) Synthesis of <b>Leu-Ile-Val</b> .....	78
3.2.3. Techniques for the characterization of the final and intermediates synthesized products.....	78
Fourier Transform Infrared Spectrometry (FT-IR) .....	78
Thermogravimetric analysis (TGA) .....	78
X-ray diffraction (XRD).....	78
High resolution transmission electron microscopy (HR-TEM) .....	78
Scanning electron microscopy (SEM).....	79
Dynamic light scattering (DLS) .....	79
Brunauer–Emmett–Teller analysis (BET).....	80
Nuclear magnetic resonance spectroscopy (RMN) .....	81
Mass spectrometry (MS) .....	81
High resolution mass spectrometry HR-MS and MALDI-FT-ICR.....	82
Fourier Transform Infrared Microscopy (FT-IR microscopy) .....	82
Magnetic measurements .....	83
Microwave irradiation .....	83
Electrical measurements of transistors based on magnetic nanoparticles .....	83
3.2.4. Determination of the bioavailability of <b>Fe<sub>3</sub>O<sub>4</sub>-PABA</b> nanoparticles using the chicken embryo chorioallantoic membrane (CAM) model and the murine model.....	83
<b>CHAPTER 4. OBJECTIVES AND ORIGINALITY .....</b>	<b>86</b>
<b>CHAPTER 5. ORIGINAL CONTRIBUTIONS REGARDING THE SYNTHESIS OF MAGNETIC NANOSTRUCTURED SYSTEMS AS SOLID SUPPORTS FOR PEPTIDE SYNTHESIS .....</b>	<b>89</b>
5.1. Objectives of experimental research .....	89
5.2. Obtaining and characterizing nanostructured systems used as solid support in solid phase peptide synthesis .....	90
5.2.1. Obtaining and characterizing of <b>Fe<sub>3</sub>O<sub>4</sub>-PABA</b> nanoparticles.....	90
Determination of the bioavailability of <b>Fe<sub>3</sub>O<sub>4</sub>-PABA</b> nanoparticles using the chicken embryo chorioallantoic membrane (CAM) model and the murine model .....	95
5.2.2. Obtaining and characterizing of <b>Fe<sub>3</sub>O<sub>4</sub>-PABA-SiO<sub>2</sub></b> magnetic nanoparticles with silica secondary shell .....	103
5.2.2.1. Obtaining and characterizing of <b>Fe<sub>3</sub>O<sub>4</sub>-PABA-SiO<sub>2</sub>-1</b> magnetic nanoparticles with silica secondary shell .....	104
5.2.2.2. Obtaining and characterizing of <b>Fe<sub>3</sub>O<sub>4</sub>-PABA-SiO<sub>2</sub>-2</b> magnetic nanoparticles with silica secondary shell .....	111
5.2.2.3. Obtaining and characterizing of <b>Fe<sub>3</sub>O<sub>4</sub>-PABA-SiO<sub>2</sub>-3</b> and <b>Fe<sub>3</sub>O<sub>4</sub>-PABA-SiO<sub>2</sub>-4</b> magnetic nanoparticles with silica secondary shell .....	113
5.2.3. Obtaining and characterizing nanostructured systems usable in solid phase synthesis.....	124
5.2.3.1. Obtaining and characterization of <b>Fe<sub>3</sub>O<sub>4</sub>-PABA-GA-PPD</b> nanostructured system.....	125

5.2.3.2. Obtaining and characterization of <b>Fe<sub>3</sub>O<sub>4</sub>-PABA-SiO<sub>2</sub>-APS-HMBA</b> nanostructured system .....	126
5.2.3.3. Obtaining and characterization of <b>Fe<sub>3</sub>O<sub>4</sub>-PABA-SiO<sub>2</sub>-SiLOH</b> nanostructured system .....	130
5.2.3.4. Obtaining and characterization of <b>Fe<sub>3</sub>O<sub>4</sub>-PABA-SiO<sub>2</sub>-SiLOHmw</b> nanostructured system .....	134
5.3. Conclusions.....	136
<b>CHAPTER 6. ORIGINAL CONTRIBUTIONS TO THE ELECTRONIC APPLICATIONS OF Fe<sub>3</sub>O<sub>4</sub>-PABA NANOPARTICLES AND THE INVESTIGATION OF THE ELECTRICAL PROPERTIES OF Fe<sub>3</sub>O<sub>4</sub>-PABA-SiO<sub>2</sub> NANOFILM DOPED WITH DPPH RADICAL .....</b>	<b>137</b>
6.1. Special applications of <b>Fe<sub>3</sub>O<sub>4</sub>-PABA</b> nanoparticles: Obtaining the transistor based on <b>Fe<sub>3</sub>O<sub>4</sub>-PABA</b> nanoparticles.....	138
6.2. Investigation of the electrical properties of <b>Fe<sub>3</sub>O<sub>4</sub>-PABA-SiO<sub>2</sub></b> nanofilm doped with <b>DPPH radical</b> .....	143
6.2.1. Characterization of the <b>Fe<sub>3</sub>O<sub>4</sub>-PABA-SiO<sub>2</sub></b> nanofilm doped with <b>DPPH radical</b> .....	147
6.3. Conclusions.....	151
<b>CHAPTER 7. ORIGINAL CONTRIBUTIONS ON PEPTIDE SYNTHESIS ON MAGNETIC NANOSTRUCTURED SUPPORT (NSS).....</b>	<b>152</b>
7.1. Objectives of experimental research.....	153
7.2. Synthesis of peptides on magnetic nanostructured support .....	153
7.2.1. Obtaining and characterizing of <b>Lys-Ala-Gly</b> .....	158
7.2.2. Obtaining and characterizing of <b>Val-Ile-Lys</b> .....	160
7.2.3. Obtaining and characterizing of <b>Gly-Ala-Phe</b> .....	163
7.2.4. Obtaining and characterizing of <b>Leu-Ile-Val</b> .....	164
7.3. Identification of peptides and possible fragments obtained by FT-MS analysis.....	166
7.3.1. Identification of <b>Lys-Ala-Gly</b> and possible fragments .....	168
7.3.2. Identification of <b>Val-Ile-Lys</b> and possible fragments .....	173
7.3.3. Identification of <b>Gly-Ala-Phe</b> and possible fragments.....	178
7.3.4. Identification of <b>Leu-Ile-Val</b> and possible fragments .....	179
7.4. Conclusions.....	184
<b>CHAPTER 8. GENERAL CONCLUSIONS.....</b>	<b>185</b>
<b>ANNEXES.....</b>	<b>188</b>
<b>BIBLIOGRAPHY .....</b>	<b>197</b>
<b>DISSEMINATION OF RESULTS .....</b>	<b>213</b>

**Keywords:** core-shell magnetic nanoparticles, linker, solid support, Fmoc, solid phase synthesis, peptide synthesis, thin-film transistor

## **II. ORIGINAL CONTRIBUTIONS**

## CHAPTER 4. OBJECTIVES AND ORIGINALITY

Solid phase peptide synthesis is one of the few synthetic methodologies that has revolutionized classical organic synthesis. Simple working procedures, which require small amounts of reagents, but also the economic value of the resulting products, offer the synthesis of peptides on solid support several advantages over classical organic synthesis.

*The main objective of this doctoral thesis consists in a new approach to the solid phase synthesis of peptides (SPPS), namely: the synthesis of peptides on magnetic nanostructured support using the Fmoc strategy. To this end, instead of the standard solid support, consisting of a functionalized resin, we have developed new types of solid supports consisting of core-shell ferrite nanoparticles with PABA, silica secondary shell and various linker systems with polar terminal grouping, labile under final cleavage conditions, capable of efficiently binding N-terminally blocked amino acids and compatible with all stages of said peptide synthesis. The ability to attach new nanostructured systems using the SPPS principle was tested by successively coupling three different amino acids protected by Fmoc.*

In order to achieve the main objective, several secondary objectives were pursued:

- (1) Synthesis and characterization of magnetic materials with organic shell constituting solid support in peptide synthesis
- (2) Synthesis and characterization of core-shell systems with silica secondary shell
- (3) Design, synthesis and characterization of linker systems with polar terminal groups
- (4) Testing of newly synthesized nanostructured systems as a solid support in solid phase synthesis of peptides
- (5) Investigation of the electrical properties of nanofilms based on magnetic nanoparticles with organic shell and nanofilms with organic shell and secondary silica shell doped with DPPH radical
- (6) Determination of bioavailability of **Fe<sub>3</sub>O<sub>4</sub>-PABA** magnetic nanoparticles

The originality of this paper lies in the development of a new method of peptide synthesis that uses as a solid support a nanostructured system consisting of magnetic nanoparticles with PABA shell (**Fe<sub>3</sub>O<sub>4</sub>-PABA**) and magnetic nanoparticles with PABA shell and silica secondary shell (**Fe<sub>3</sub>O<sub>4</sub>-PABA-SiO<sub>2</sub>**) functionalized with different linker systems. Thus, new linker systems and new solid supports were developed.

**Chapter 5** presents the original contribution on the methods of synthesis of nanostructured systems based on magnetic nanoparticles with organic shell (PABA) and silica



secondary shell used as solid support in the synthesis of peptides on solid support: **Fe<sub>3</sub>O<sub>4</sub>-PABA-GA-PPD**, **Fe<sub>3</sub>O<sub>4</sub>-PABA-SiO<sub>2</sub>-APS-HMBA**, **Fe<sub>3</sub>O<sub>4</sub>-PABA-SiO<sub>2</sub>-SiL-OH** and **Fe<sub>3</sub>O<sub>4</sub>-PABA-SiO<sub>2</sub>-SiL-OH<sub>mw</sub>**. Also, this chapter presents the design and synthesis methods of the new linkers tested in peptide synthesis.

The results obtained were published in the articles:

**Alina Moroşan**, Dan Eduard Mihaiescu, Daniela Istrati, Georgeta Voicu, Adrian Fudulu, Raluca Stan, „Polar shell magnetic nanostructured systems for heterogeneous nanophase reactions”, *U.P.B. Sci. Bull*, **2018**, 80 (3), 53-64, ISSN 1454-2331

**Alina Moroşan**, Dan Eduard Mihaiescu, Daniela Istrati, Georgeta Voicu, Mihai Radu, Anamaria Hanganu, Raluca Stan, „Functionalized silica shell magnetic nanoparticles for nanophase peptide synthesis applications”, *Microporous and Mesoporous Materials*, **2019**, 286, 45-56. (IF = 4.551)

Also, in this chapter, the bioavailability of magnetic nanoparticles was determined **Fe<sub>3</sub>O<sub>4</sub>-PABA** using the chicken embryo chorioallantoic membrane (CAM) model and the murine model.

**Chapter 6** contains the results obtained after the investigation of the electrical properties of nanofilms based on magnetic nanoparticles with organic shell, as well as of nanofilms with organic shell and secondary shell of silica doped with DPPH radical.

The results obtained were published in the article:

Cristian Ravariu, Dan Eduard Mihaiescu, **Alina Morosan**, Daniela Istrati, Bogdan Purcăreanu, Rodica Cristescu, Roxana Truşcă, Bogdan Ştefan Vasile, „Solution for green organic thin film transistors: Fe<sub>3</sub>O<sub>4</sub> nano-core with PABA external shell as p-type film”, *Journal of Materials Science: Materials in Electronics*, **2020**, 31, 1-11. (IF = 2.220)

Into the **Chapter 7** a new approach to peptide synthesis is presented using the principle of solid support peptide synthesis, namely: peptide synthesis on magnetic nanostructured support. Thus, instead of the standard polymeric solid support, we have developed new types of solid support consisting of core-shell ferrite nanoparticles with PABA, silica secondary shell and various linker systems with polar terminal group, labile in the final cleavage conditions, capable to efficiently bind N-terminally blocked amino acids and compatible with all stages of peptide synthesis. The new synthesized nanostructured systems have been successfully tested by successively coupling three different Fmoc-protected amino acids. Synthesized peptides (**Lys-Ala-Gly**, **Val-Ile-Lys**, **Gly-Ala-Phe**, **Leu-Ile-Val**) were identified using advanced analysis techniques, LC-MS and HR-MS mass spectrometry. The structure of the synthesized peptides was confirmed by identifying fragmentation ions in the MS spectra.

## CHAPTER 5. ORIGINAL CONTRIBUTIONS REGARDING SYNTHESIS OF SYSTEMS MAGNETIC NANOSTRUCTURES AS SOLID SUPPORTS FOR PEPTIDE SYNTHESIS

### Objectives of experimental research:

- (1) Obtaining and characterizing magnetic nanoparticles with PABA shell. Determination of bioavailability of magnetic nanoparticles **Fe<sub>3</sub>O<sub>4</sub>-PABA** using the chicken embryo chorioallantoic membrane (CAM) model and the murine model.
- (2) Obtaining and characterizing magnetic nanoparticles with silica secondary shell and of nanostructured systems used as a solid support in peptide synthesis.

### 5.2. Obtaining and characterizing nanostructured systems used as a solid support in the solid phase peptides synthesis

#### 5.2.1. Obtaining and characterizing nanoparticles *Fe<sub>3</sub>O<sub>4</sub>-PABA*

Core-shell magnetic nanoparticles (**Fe<sub>3</sub>O<sub>4</sub>-PABA**) were synthesized by the coprecipitation method [59, 78, 136, 138]. This method is very simple and economical, the size and shape of the nanoparticles obtained depend on the type of salts used, dilution, the ratio of Fe<sup>3+</sup> and Fe<sup>2+</sup>, pH value, reaction temperature, stirring speed. As the affinity of magnetic nanoparticles for acidic groups is known [150], was selected *para*-aminobenzoic acid (PABA) showing –NH<sub>2</sub> groups available after nanoparticle bonding to facilitate silica coating. The choice of acid *para*-aminobenzoic acid is also based on its biological properties that give this type of magnetic nanoparticles good biocompatibility, widening their area of application.

Chemical reaction of Fe<sub>3</sub>O<sub>4</sub> nanoparticles formation:

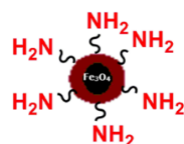
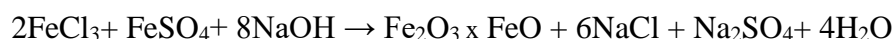


Figure 5.1. Schematic representation of **Fe<sub>3</sub>O<sub>4</sub>-PABA** nanoparticles

The crystal structure of the magnetic core of **Fe<sub>3</sub>O<sub>4</sub>-PABA** nanoparticles was demonstrated by XRD and SAED analysis; and their hydrodynamic size and morphology through DLS, TEM and SEM.

Hydrodynamic diameter of **Fe<sub>3</sub>O<sub>4</sub>-PABA** nanoparticles according to DLS is 71 nm. The value of the obtained polydispersity index, 0.191 proves a good uniformity and the good stability of the dispersion is proved by the value of the zeta potential, + 51.6 mV, due to the PABA shell by the presence of the -NH<sub>3</sub><sup>+</sup> groups.

Morphology of **Fe<sub>3</sub>O<sub>4</sub>-PABA** nanoparticles was determined by electron microscopy. In the SEM images we can observe a granular morphology with a good homogeneity.

TEM images (Fig. 5.5) confirm the presence of **Fe<sub>3</sub>O<sub>4</sub>-PABA** nanoparticles with a core size of approximately 12 nm. SAED image (Selected Area Electron Diffraction) confirms the presence of the crystalline structure of Fe<sub>3</sub>O<sub>4</sub>. The use of DLS and TEM complementary methods allows the differentiation between the hydrodynamic diameter of the core-shell / shell system solvation, respectively of the magnetic core of Fe<sub>3</sub>O<sub>4</sub>.

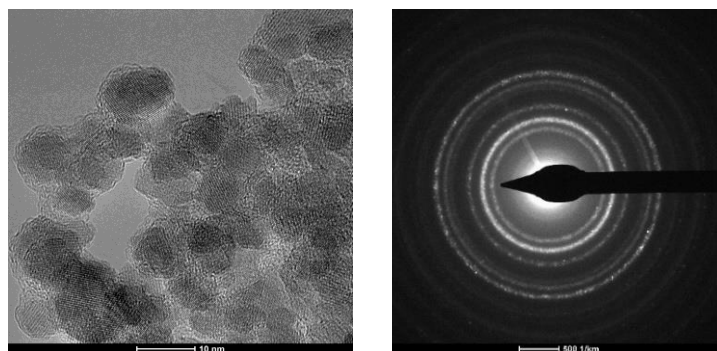


Figure 5.5. TEM and SAED images for **Fe<sub>3</sub>O<sub>4</sub>-PABA**

The elemental composition of **Fe<sub>3</sub>O<sub>4</sub>-PABA** nanoparticles performed by energy dispersive X-ray spectroscopy (EDX) shows that the elements Fe, O, C and N are predominant in test, confirming the presence of elements in the Fe<sub>3</sub>O<sub>4</sub>-PABA core-shell system. The presence of Cu is due to the support grid that was used to perform the analysis [151].

The specific surface area of the **Fe<sub>3</sub>O<sub>4</sub>-PABA** nanoparticles was estimated by BET analysis. According to the BET analysis, the obtained material has a specific surface of 653 m<sup>2</sup>/g, with pore size dBJH=2.38 nm and pore volume Vp=0.74 cm<sup>3</sup>/g.

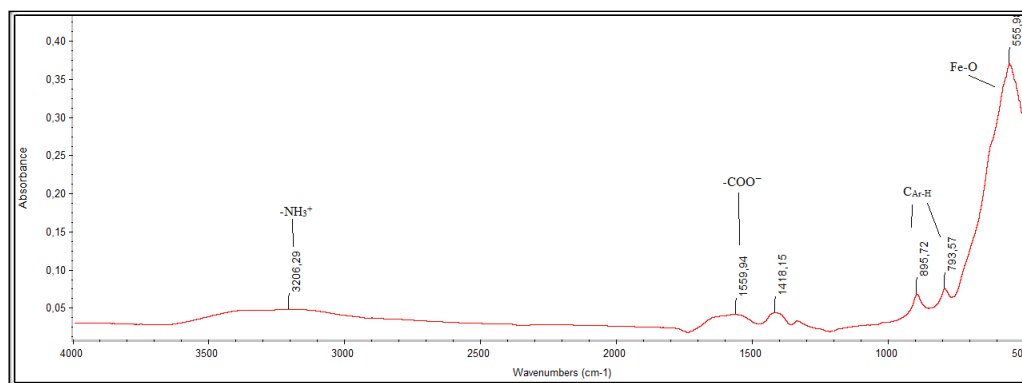


Figure 5.7. FT-IR spectrum for **Fe<sub>3</sub>O<sub>4</sub>-PABA**

The existence of the PABA shell was confirmed by the FT-IR spectrum (Fig. 5.7) through the presence of characteristic bands for the  $-\text{NH}_3^+$  at  $3206\text{ cm}^{-1}$  and stretching vibration characteristic of the carboxylate at  $1559\text{ cm}^{-1}$ . Aromatic structure of the acid *p*-aminobenzoic acid is highlighted by the presence of characteristic bands in the range  $793\text{--}895\text{ cm}^{-1}$ . Fe-O bond vibrations that can be observed at  $555\text{ cm}^{-1}$  confirms the presence of magnetite.

Magnetic properties of **Fe<sub>3</sub>O<sub>4</sub>-PABA** nanoparticles were measured using a vibrating sample magnetometer (VSM). The magnetization curve can be seen in Fig. 5.10, as well as the value of saturation magnetization  $M_s = 63.174\text{ emu/g}$ . The nanoparticles obtained were efficiently separated using an external magnetic field which shows that the PABA shell does not affect the magnetic properties and their use in subsequent applications.

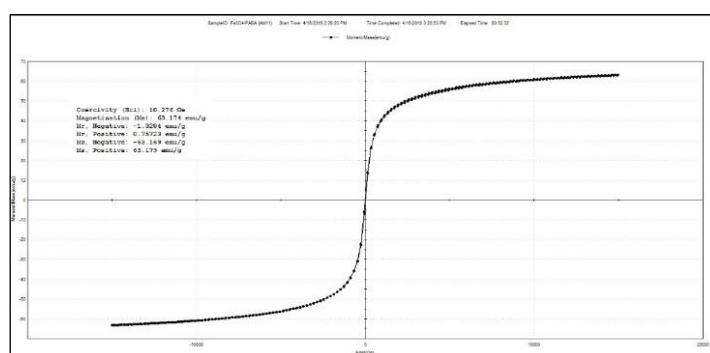


Figure 5.10. Magnetization curve of **Fe<sub>3</sub>O<sub>4</sub>-PABA** nanoparticles

### ***Determination of bioavailability of Fe<sub>3</sub>O<sub>4</sub>-PABA nanoparticles using the model chorioallantoic membrane (CAM) of chicken embryo and murine model***

Preliminary studies on models *in vivo* were performed on the model of the chorioallantoic membrane of chicken embryos and on the murine model, using **Fe<sub>3</sub>O<sub>4</sub>-PABA** magnetic nanoparticles within the Laboratory for experimental animal studies, Biobase of the University of Medicine and Pharmacy of Craiova. In order to test the biological properties and potential biomedical perspectives of **Fe<sub>3</sub>O<sub>4</sub>-PABA** the persistence in circulation, the embolic potential after intravenous administration, and the possibility of targeted conduction of nanoparticles using an external static magnetic field were tested.

#### ***Testing on the model of the chorioallantoic membrane***

To test the nanoparticles persistence in the circulation, an attempt was made to aggregate them intravascularly in a static magnetic field, by applying a strong magnet to the surface of the chorioallantoic membrane. The persistence of nanoparticles in circulation correlates with the amount of nanoparticles aggregated in the area of action of the magnetic field. The data obtained showed that the size of intravascular deposits made by intravascular aggregation of PABA-

functionalized ferromagnetic nanoparticles do not depend on the time the eggs were kept in the incubator after injection, but on the time of exposure to the action of the static magnetic field.

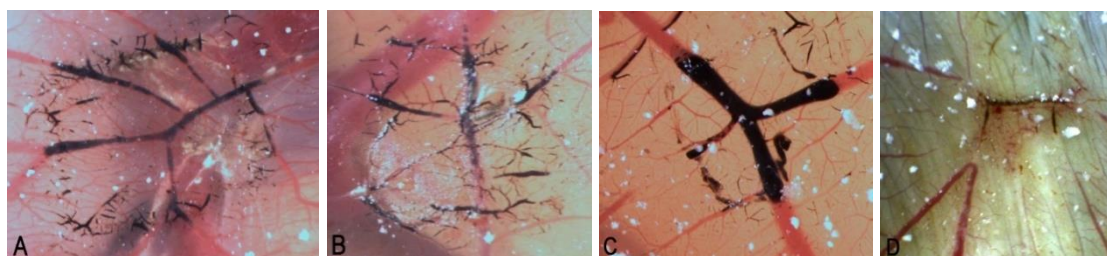


Figure 5.13. Intravascular aggregation of **Fe<sub>3</sub>O<sub>4</sub>-PABA** nanoparticles after exposure for 30 minutes to the action of a static magnetic field. D - appearance of the chorioallantoic membrane 24 hours after blockage magnetic field of a large caliber vessel.

The normal development of embryos after performing these experiments can be considered a strong argument in favor of a reduced embolic potential of nanoparticle aggregates formed intravascularly under the action of the magnetic field, as well as for the reduced teratogenic potential of PABA-functionalized ferromagnetic nanoparticles.

#### *Testing on the murine model*

For this test, two white Wistar rats were used, in which the 1 mL dose of the dispersion of PABA-functionalized ferromagnetic nanoparticles was injected through the tail vein, respectively into the superior mesenteric vein (after laparotomy).

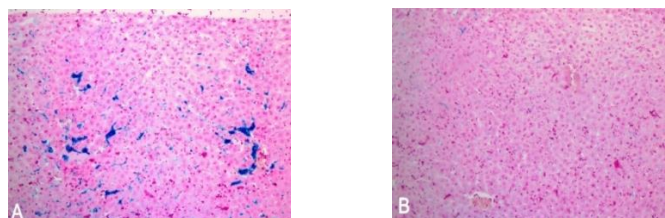


Figure 5.18. Appearance of the deposits of ferromagnetic nanoparticles (blue colored) at the level of the veins in the portal spaces in the area exposed to the action of the magnetic field (A) and in an unexposed area (B).  
*Injection at the level superior mesenteric vein. Prussian blue coloring. Ob x10.*

Histological analysis of Prussian blue colored sections, a technique that is very sensitive to Fe<sup>3+</sup> deposits highlighted rich nanoparticle deposits in the veins of the port space in the area of the liver parenchyma exposed to the action of the external static magnetic field (Fig. 5.18 A). At the level of the veins in the gate spaces of the areas not exposed to the magnetic field or discrete deposits of ferromagnetic nanoparticles were observed (Fig. 5.18 B).

Conclusions of this experiment:

- the PABA shell allows persistence in circulation and easy handling under the action of a static magnetic field of the ferromagnetic nanoparticles it functions.
- nanoparticles of the type **Fe<sub>3</sub>O<sub>4</sub>-PABA** are biocompatible and have a low risk of intravenous embolism

### 5.2.2. Obtaining and characterizing $Fe_3O_4$ -PABA- $SiO_2$ magnetic nanoparticles with secondary silica shell

Coating the surface of  $Fe_3O_4$ -PABA nanoparticles with silica, by the presence of abundant silanol groups on the surface of the nanoparticles allows an easy and efficient subsequent functionalization [167].

The  $Fe_3O_4$ -PABA- $SiO_2$  nanoparticles were obtained by a modified sol-gel method using two sources of silica, namely: a solution of sodium silicate,  $\rho=1.39 \text{ g mL}^{-1}$  and TEOS. The  $NH_4OH$  was used as the alkaline agent and as surfactant: CTAB (Table 5.1.).

Table 5.1. Synthesis of magnetic nanoparticles with silica shell:  $Fe_3O_4$ -PABA- $SiO_2$

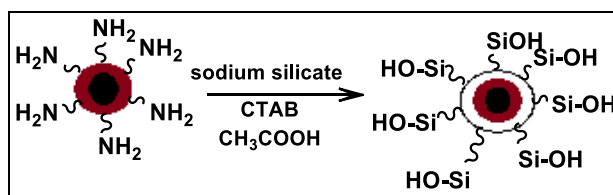
Magnetic nanoparticles with silica shell	Synthesis conditions	Silica Precursor	Alkaline agent	Template	Template removal
$Fe_3O_4$ -PABA- $SiO_2$ -1	R.T. (dripping)	Sodium silicate solution ( $\rho=1.39 \text{ g mL}^{-1}$ )	-	CTAB	Calcination $540^\circ\text{C}/24$ hours
$Fe_3O_4$ -PABA- $SiO_2$ -2	R.T. (dripping)	TEOS	$NH_4OH$	CTAB	Washing EtOH; ACN
$Fe_3O_4$ -PABA- $SiO_2$ -3	microwave (reflux)	TEOS	$NH_4OH$	CTAB	Calcination $450^\circ\text{C}/24$ hours
$Fe_3O_4$ -PABA- $SiO_2$ -4	microwave (reflux)	TEOS	$NH_4OH$	CTAB	Washing EtOH:Ac.OH 5%; EtOH

The study of the template removal process was performed by two methods:

- calcination at temperatures of  $450^\circ\text{C}$  and  $540^\circ\text{C}/24$  hours;
- repeated washings with ultrapure water and organic solvents of different polarities: MeOH, acetone, DCM, EtOH/5% Acetic acid and EtOH.

#### 5.2.2.1. Obtaining and characterizing $Fe_3O_4$ -PABA- $SiO_2$ -1 magnetic nanoparticles with secondary silica shell that used a sodium silicate solution as a silica source

For the synthesis of magnetic nanoparticles with PABA shell and silica secondary shell for which a sodium silicate solution was used as the silica source, several concentrations of silica precursor (Table 5.2) were used in order to obtain a specific surface area. as high as possible [138].



Scheme 5.1. Synthesis of  $Fe_3O_4$ -PABA- $SiO_2$ -1 nanoparticles using sodium silicate solution as silica source

Table 5.2. Synthesis of magnetic nanoparticles with PABA shell and silica secondary shell for which a sodium silicate solution was used as the silica source

Sample	Sodium silicate solution ( $\rho=1.39 \text{ g mL}^{-1}$ )	Acetic Acid	Characterization
1	3.6 mL	20 mL	FT-IR, BET
2	7.2 mL	20 mL	FT-IR
3	14.4 mL	20 mL	FT-IR, BET, XRD, TEM, SEM, EDX
4	21.6 mL	20 mL	FT-IR
5	36 mL	50 mL	FT-IR
6	50.5 mL	70 mL	FT-IR
7	72 mL	100 mL	FT-IR

The optimal solution was chosen considering the following criteria, namely: the use of a small amount of silicate to prevent the tendency to agglomeration and to avoid subsequent dispersibility problems. It was also aimed at obtaining a specific area as high as possible.

The structure and morphology of **Fe<sub>3</sub>O<sub>4</sub>-PABA-SiO<sub>2</sub>-1** nanoparticles obtained (sample 3) was determined by the following techniques: FT-IR, XRD, SEM, TEM, EDX. A TGA analysis was performed to determine the heat treatment regime. The specific surface area of the material obtained was estimated by BET analysis.

Semi-quantitative X-ray diffraction analysis was performed for both the sample **3-Fe<sub>3</sub>O<sub>4</sub>-PABA-SiO<sub>2</sub>-1** before and after heat treatment. The obtained diffraction interferences prove that the **Fe<sub>3</sub>O<sub>4</sub>-PABA** nanoparticles (Fig. 5.20) retains its crystalline characteristics even after coating with silica [62]. Also, a small bit wide that can be attributed to amorphous SiO<sub>2</sub> according to data from the literature [65].

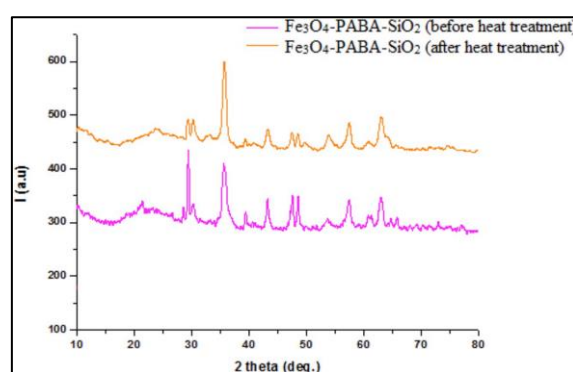


Figure 5.20. Diffractogram for the **3-Fe<sub>3</sub>O<sub>4</sub>-PABA-SiO<sub>2</sub>-1** sample before and after heat treatment

The presence of silica shell on the surface of the **3-Fe<sub>3</sub>O<sub>4</sub>-PABA-SiO<sub>2</sub>-1** nanoparticles before and after heat treatment was confirmed in the FT-IR spectrum by the presence vibrations of asymmetric stretching of Si-O-Si bonds at 1057 cm<sup>-1</sup>, respectively 1051 cm<sup>-1</sup> [107, 141] and the band corresponding to the Si-OH bond at 794 cm<sup>-1</sup>, respectively 802 cm<sup>-1</sup>. The characteristic

magnetite band corresponding to the Fe-O bond was identified at  $557\text{ cm}^{-1}$ , respectively  $556\text{ cm}^{-1}$ .

The morphology of the nanoparticles determined by SEM and TEM confirms the silica coating of the **Fe<sub>3</sub>O<sub>4</sub>-PABA** nanoparticles. SEM images show a globular morphology with good homogeneity. In the TEM images (Fig. 5.23) it can be seen that the coating of the nanoparticle surface with the secondary silica shell is uneven due to the presence of conglomerates in which magnetic nanoparticles are included in the silica structure.

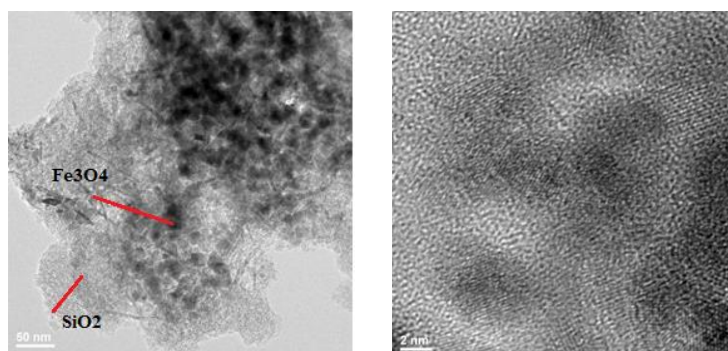


Figure 5.23. TEM images for the **3-Fe<sub>3</sub>O<sub>4</sub>-PABA-SiO<sub>2</sub>-1** sample

The elemental composition of **Fe<sub>3</sub>O<sub>4</sub>-PABA-SiO<sub>2</sub>-1** nanoparticles (sample 3) performed by energy dispersive X-ray spectroscopy (EDX) shows that the elements Fe, Si, O and C are majority in the sample, confirming the presence of elements in the **Fe<sub>3</sub>O<sub>4</sub>-PABA-SiO<sub>2</sub>-1** core-shell system. The presence of Cu is due to the support grid that was used to perform the analysis [151].

The specific surface area of **3-Fe<sub>3</sub>O<sub>4</sub>-PABA-SiO<sub>2</sub>-1** was estimated by BET analysis obtaining a specific area of  $601\text{ m}^2/\text{g}$  with pore size  $\text{dBJH}=2.25\text{ nm}$ ,  $3.7\text{ nm}$ ,  $6.3\text{ nm}$  and pore volume  $V_p=1.12\text{ cm}^3/\text{g}$ , which demonstrates the existence of a mesoporous structure of the silica secondary shell. BET analysis shows that by coating with silica of **Fe<sub>3</sub>O<sub>4</sub>-PABA** nanoparticles their specific surface area decreases. This is explained by the tendency of agglomeration of nanoparticles that occurs during heat treatment (according to TEM images- Fig. 5.23). It is observed that the variation of the amount of sodium silicate used in the synthesis does not lead to a significant change in the specific surface.

Magnetic properties of **Fe<sub>3</sub>O<sub>4</sub>-PABA-SiO<sub>2</sub>-1** nanoparticles were measured using a vibrating sample magnetometer (VSM). The magnetization curves can be seen in Figs. 5.27, as well as the value of the saturation magnetization  $M_s = 42.111\text{ emu/g}$ . The nanoparticles obtained were efficiently separated by an external magnetic field which proves that silica coating does not affect the magnetic properties of nanoparticles with applications in solid phase synthesis.



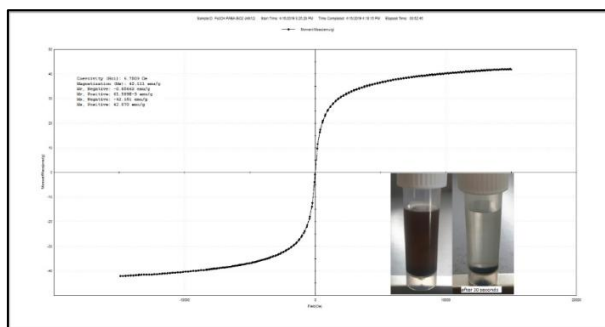
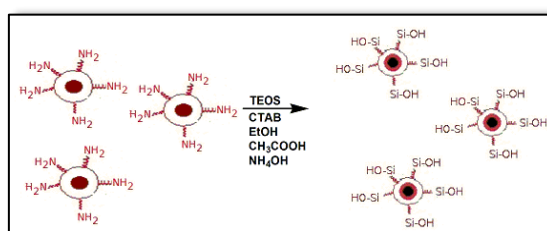


Figure 5.27. Magnetization curve and separation process of **Fe<sub>3</sub>O<sub>4</sub>-PABA-SiO<sub>2</sub>-1** nanoparticles using an external magnetic field

#### 5.2.2.2. Obtaining and characterizing of **Fe<sub>3</sub>O<sub>4</sub>-PABA-SiO<sub>2</sub>-2** magnetic nanoparticles with secondary silica shell

To achieve an improvement in the properties of core-shell nanoparticles for synthesis of **Fe<sub>3</sub>O<sub>4</sub>-PABA-SiO<sub>2</sub>-2** a modified sol-gel method was adopted at room temperature, by dropwise addition and magnetic stirring, using TEOS as the silica precursor, NH<sub>4</sub>OH as alkaline agent and CTAB as surfactant.



Scheme 5.3. Synthesis of **Fe<sub>3</sub>O<sub>4</sub>-PABA-SiO<sub>2</sub>-2** nanoparticles using TEOS as silica source

The presence of silica shell on the surface of Fe<sub>3</sub>O<sub>4</sub>-PABA nanoparticles before and after removal of the template by washing with EtOH, was confirmed by recording the FT-IR spectrum which highlighted characteristic bands as follows:

- asymmetric stretching vibrations of the Si–O–Si bonds at 1006 cm<sup>-1</sup>, respectively 1012 cm<sup>-1</sup>;
- asymmetric tensile vibrations of the Si-OH bond at 864 cm<sup>-1</sup>, respectively 865 cm<sup>-1</sup>;
- the characteristic band of the magnetite attributed to the Fe – O bond was identified at 534 cm<sup>-1</sup>, respectively 558 cm<sup>-1</sup>.

The morphology of **Fe<sub>3</sub>O<sub>4</sub>-PABA-SiO<sub>2</sub>-2** nanoparticles was determined by examining TEM micrographs (Fig. 5.29). The obtained images confirm the presence of the secondary silica shell and a low tendency of agglomeration can be observed, which explains the increased dispersibility in common solvents used in peptide synthesis.

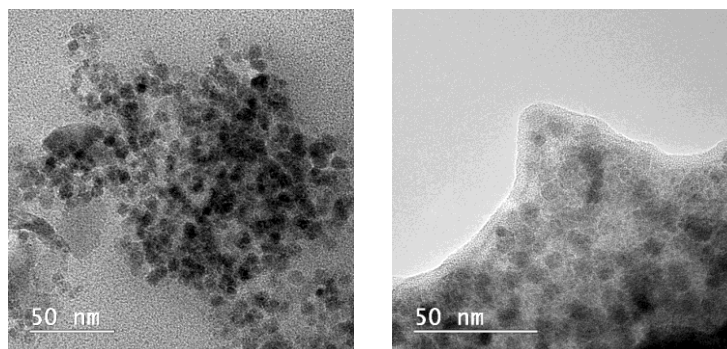
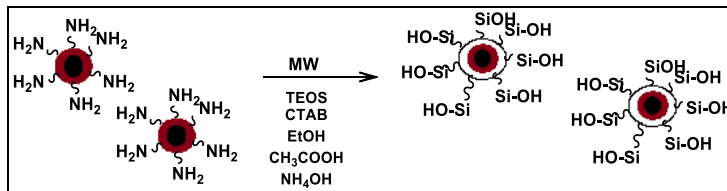


Figure 5.29. TEM images for **Fe<sub>3</sub>O<sub>4</sub>-PABA-SiO<sub>2</sub>-2**

The magnetic properties of **Fe<sub>3</sub>O<sub>4</sub>-PABA-SiO<sub>2</sub>-2** were measured using a vibrating sample magnetometer (VSM) obtaining a value of saturation magnetization  $M_s = 6.791$  emu/g. The nanoparticles obtained by this method were also efficiently separated by an external magnetic field.

#### 5.2.2.3. Obtaining and characterizing of **Fe<sub>3</sub>O<sub>4</sub>-PABA-SiO<sub>2</sub>-3** and **Fe<sub>3</sub>O<sub>4</sub>-PABA-SiO<sub>2</sub>-4** magnetic nanoparticles with secondary silica shell that used TEOS as a silica source

The synthesis of **Fe<sub>3</sub>O<sub>4</sub>-PABA-SiO<sub>2</sub>-3** and **Fe<sub>3</sub>O<sub>4</sub>-PABA-SiO<sub>2</sub>-4** was performed by a modified sol-gel method in the microwave field.



Scheme 5.5. The synthesis of **Fe<sub>3</sub>O<sub>4</sub>-PABA-SiO<sub>2</sub>-3** and **Fe<sub>3</sub>O<sub>4</sub>-PABA-SiO<sub>2</sub>-4**

For the **Fe<sub>3</sub>O<sub>4</sub>-PABA-SiO<sub>2</sub>-3** sample the template was removed by calcination at 450 °C for 24 hours, and for the **Fe<sub>3</sub>O<sub>4</sub>-PABA-SiO<sub>2</sub>-4** sample the template was removed by washing with EtOH: 5 % acetic acid, followed by washing with EtOH.

The structure and morphology of **Fe<sub>3</sub>O<sub>4</sub>-PABA-SiO<sub>2</sub>-3** and **Fe<sub>3</sub>O<sub>4</sub>-PABA-SiO<sub>2</sub>-4** nanoparticles was investigated by the following techniques: FT-IR, TEM, SAED, EDX.

In order to establish the heat treatment regime for the **Fe<sub>3</sub>O<sub>4</sub>-PABA-SiO<sub>2</sub>** sample, a TGA analysis was performed and it was found that washing with organic solvent removes the CTAB template to a greater extent than washing with water, a fact visible by the loss of superior mass (in the case of washing with water) in the range 190-500 °C when a larger amount of substance is oxidized.

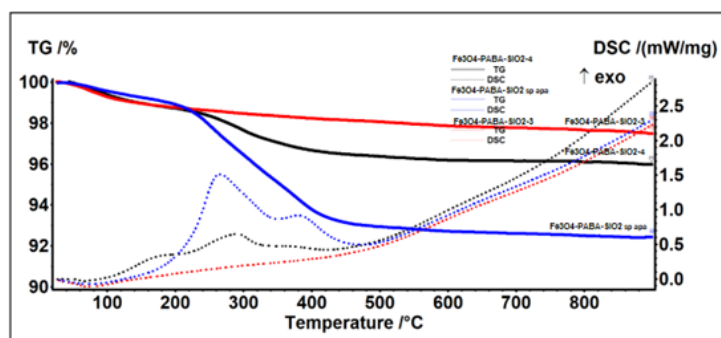


Figure 5.34. Comparative TGA analysis performed after the water washing step of **Fe<sub>3</sub>O<sub>4</sub>-PABA-SiO<sub>2</sub>**, respectively of **Fe<sub>3</sub>O<sub>4</sub>-PABA-SiO<sub>2</sub>-3** and **Fe<sub>3</sub>O<sub>4</sub>-PABA-SiO<sub>2</sub>-4**

The residue of all samples analysed by TGA did not change color compared to the initial sample and showed magnetic properties. It was observed that there is no specific physical transformation of maghemite-hematite in the range of 300-500°C [173], which confirms the presence of the silica secondary shell.

The specific surface area of **Fe<sub>3</sub>O<sub>4</sub>-PABA-SiO<sub>2</sub>-3** and **Fe<sub>3</sub>O<sub>4</sub>-PABA-SiO<sub>2</sub>-4** was estimated by BET analysis. For the **Fe<sub>3</sub>O<sub>4</sub>-PABA-SiO<sub>2</sub>-3** sample a specific surface area of 127 m<sup>2</sup>/g with pore size d<sub>BJH</sub>=33.223 nm and pore volume V<sub>p</sub>=0.690 cm<sup>3</sup>/g, and for **Fe<sub>3</sub>O<sub>4</sub>-PABA-SiO<sub>2</sub>-4** a specific surface area of 122 m<sup>2</sup>/g with pore size d<sub>BJH</sub>=19.497 nm and pore volume V<sub>p</sub>=0.595 cm<sup>3</sup>/g. The procedure for removing the template for samples synthesized in the microwave field does not significantly affect the specific surface and the pore volume, respectively.

a) Characterization of **Fe<sub>3</sub>O<sub>4</sub>-PABA-SiO<sub>2</sub>-3** nanoparticles with secondary silica shell

The presence of silica shell for **Fe<sub>3</sub>O<sub>4</sub>-PABA-SiO<sub>2</sub>-3** nanoparticles for which TEOS was used as a silica source was confirmed by recording the FT-IR spectrum in which the presence of the band characteristic for asymmetric Si-O-Si stretching vibrations at 1049 cm<sup>-1</sup> was identified. The characteristic band of magnetite can be observed at 551 cm<sup>-1</sup> corresponding to the Fe-O bond.

The morphology of **Fe<sub>3</sub>O<sub>4</sub>-PABA-SiO<sub>2</sub>-3** nanoparticles was determined by TEM (Fig. 5.40). Analysing the obtained micrographs, the presence of the silica shell with a thickness of approx. 2 nm. Also, in the TEM images it can be seen that by calcination, the nanoparticles tend to agglomerate. The SAED image confirms the crystal structure of Fe<sub>3</sub>O<sub>4</sub>.

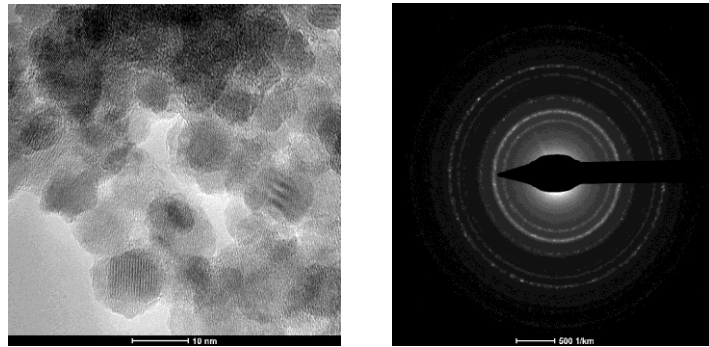


Figure 5.40. TEM and SAED images for **Fe<sub>3</sub>O<sub>4</sub>-PABA-SiO<sub>2</sub>-3**

The elemental composition of **Fe<sub>3</sub>O<sub>4</sub>-PABA-SiO<sub>2</sub>-3** nanoparticles made by Energy dispersive X-ray spectroscopy (EDX) shows that the elements Fe, Si, O, C and N are the majority in the sample, confirming the presence of elements in the **Fe<sub>3</sub>O<sub>4</sub>-PABA-SiO<sub>2</sub>-3** core-shell system. The presence of Cu is due to the support grid that was used to perform the analysis [151].

b) Characterization of **Fe<sub>3</sub>O<sub>4</sub>-PABA-SiO<sub>2</sub>-4** nanoparticles with secondary silica shell

The presence of silica shell for **Fe<sub>3</sub>O<sub>4</sub>-PABA-SiO<sub>2</sub>-4** nanoparticles was confirmed by recording the FT-IR spectrum by the presence of the band characteristic for asymmetric stretching vibrations of Si-O-Si at 1064 cm<sup>-1</sup>. The presence of magnetite is highlighted by the characteristic band at 553 cm<sup>-1</sup> corresponding to the Fe-O bond.

TEM analysis of **Fe<sub>3</sub>O<sub>4</sub>-PABA-SiO<sub>2</sub>-4** nanoparticles (Fig. 5.43) confirms the presence of the silica shell with a thickness of approx. 2 nm and a lower agglomeration tendency. The crystal structure of Fe<sub>3</sub>O<sub>4</sub> is confirmed by the SAED image.

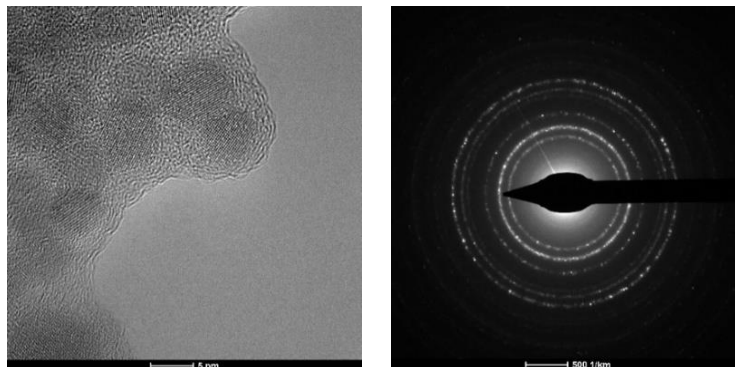


Figure 5.43. TEM and SAED images for **Fe<sub>3</sub>O<sub>4</sub>-PABA-SiO<sub>2</sub>-4**

The elemental composition of **Fe<sub>3</sub>O<sub>4</sub>-PABA-SiO<sub>2</sub>-4** nanoparticles made by Energy dispersive X-ray spectroscopy (EDX) shows that the elements Fe, Si, O, C and N are the majority in the sample, confirming the presence of elements in the **Fe<sub>3</sub>O<sub>4</sub>-PABA-SiO<sub>2</sub>-4** core-shell system. The presence of Cu is due to the support grid that was used to perform the analysis [151].

The magnetic properties of **Fe<sub>3</sub>O<sub>4</sub>-PABA-SiO<sub>2</sub>-4** nanoparticles were measured using a vibrating sample magnetometer (VSM), obtaining a value of saturation magnetization  $M_s = 57.121$  emu/g. The nanoparticles obtained by this method were also efficiently separated using an external magnetic field.

### 5.2.3. Obtaining and characterizing nanostructured systems usable in solid phase synthesis

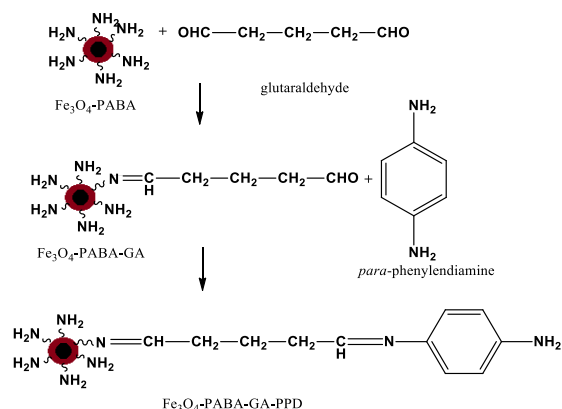
Resins used as a solid support in peptide synthesis must have a high capacity and allow easy purification by filtration. For commonly used resins, the accessibility of grafted functionalities requires the inflation of particles, and the diffusion of reagents into the microgel is limited. Nanoparticles overcome this problem, e.g. nanoparticles of  $\sim 70$  nm have an area of  $\sim 1.1 \times 10^5$  times higher and has improved accessibility to surface functionalities through direct access to the reaction center. Also, magnetic sedimentation ensures easy purification after each reaction step [26].

In this paper they were designed and tested as solid support for peptide synthesis through the Fmoc strategy **nanostructured systems based on core-shell ferrite nanoparticles with PABA shell, silica secondary shell, and various linker systems with -NH<sub>2</sub> terminal groups or -CH<sub>2</sub>-OH free** suitable for attaching Fmoc protected amino acids. The methods for obtaining and characterizing these systems are presented below.

#### 5.2.3.1. Obtaining and characterization of **Fe<sub>3</sub>O<sub>4</sub>-PABA-GA-PPD** nanostructured system

The first designed nanostructured system is based on a new concept using core-shell magnetic nanoparticles, **Fe<sub>3</sub>O<sub>4</sub>-PABA** and an ambident linker system with grouping -NH<sub>2</sub> free, compatible with all stages of synthesis. For this purpose, glutaraldehyde (GA) was chosen as the linker due to its easy coupling to amino groups. Also, to get a group -NH<sub>2</sub> reactive at the end of the linker system (Scheme 5.7.), capable of efficiently binding N-terminal blocked amino acids, grafted *p*-phenylenediamine (PPD) [136].

The presence of grafted glutaraldehyde on the surface of **Fe<sub>3</sub>O<sub>4</sub>-PABA** nanoparticles and subsequent attachment of *p*-phenylenediamine was confirmed by FT-IR spectrometry. Thus, in the comparative FT-IR spectrum **Fe<sub>3</sub>O<sub>4</sub>-PABA-GA** and **Fe<sub>3</sub>O<sub>4</sub>-PABA-GA-PPD** (Figure 5.46) can be observed the attachment of GA by an azomethine bond demonstrated by the presence of absorption bands characteristic of the -CH=N at  $1630\text{ cm}^{-1}$  and unreacted formyl group at  $1718\text{ cm}^{-1}$ .



Scheme 5.7. Nanostructured core-shell linker system: **Fe<sub>3</sub>O<sub>4</sub>-PABA-GA-PPD**

The reaction with PPD led to an increase in the intensity of the band for  $-\text{CH}=\text{N}$ , confirmed by the disappearance of the band characteristic for aldehyde. PPD attachment is also confirmed by the presence of absorption bands characteristic of the  $-\text{NH}_2$  terminal group at  $3372\text{ cm}^{-1}$  and  $3298\text{ cm}^{-1}$ .

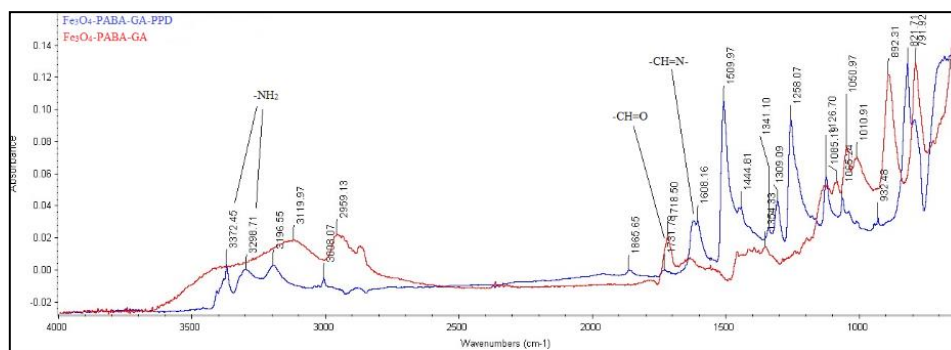
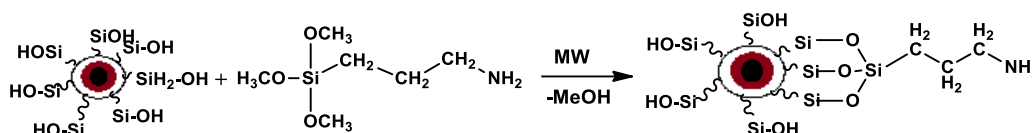


Figure 5.46. Comparative FT-IR spectrum: **Fe<sub>3</sub>O<sub>4</sub>-PABA-GA** and **Fe<sub>3</sub>O<sub>4</sub>-PABA-GA-PPD**

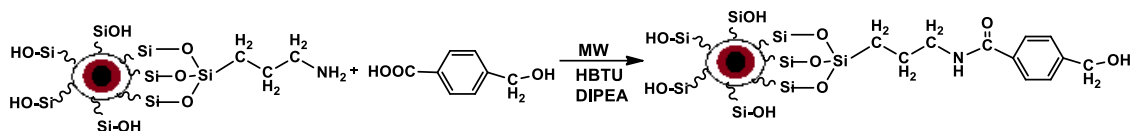
### 5.2.3.2. Obtaining and characterization of the **Fe<sub>3</sub>O<sub>4</sub>-PABA-SiO<sub>2</sub>-APS-HMBA** nanostructured system

For the functionalization of **Fe<sub>3</sub>O<sub>4</sub>-PABA-SiO<sub>2</sub>-3** and **Fe<sub>3</sub>O<sub>4</sub>-PABA-SiO<sub>2</sub>-4** magnetic nanoparticles with secondary silica shell, 3-aminopropyltrimethoxysilane (APTMS) was used in order to obtain free reactive  $-\text{NH}_2$  groups [170] that allow the attachment subsequent linkers characteristic of solid phase synthesis of peptides.



Scheme 5.8. Synthesis of **Fe<sub>3</sub>O<sub>4</sub>-PABA-SiO<sub>2</sub>-APS**

A labile linker most commonly used in solid support peptide synthesis is 4-(Hydroxymethyl)benzoic acid (HMBA).



Scheme 5.9. Synthesis of the **Fe<sub>3</sub>O<sub>4</sub>-PABA-SiO<sub>2</sub>-APS-HMBA** nanostructured system

The advantage of using HMBA as a linker is its remanence on the solid support after cleavage of peptides with TFA which allows the characterization and subsequent use of the synthesized peptide.

The functionalization with APTMS of **Fe<sub>3</sub>O<sub>4</sub>-PABA-SiO<sub>2</sub>-3** nanoparticles was confirmed by the FT-IR spectrum by the presence of absorption bands characteristic of the free -NH<sub>2</sub> group at 3361 and 3202 cm<sup>-1</sup> and of the band corresponding to the stretching vibration C-H at 2931 cm<sup>-1</sup>. Also, the bands characteristic of asymmetric stretching vibrations of Si-O-Si at 1032 cm<sup>-1</sup> can be observed; and the band characteristic of magnetite can be observed at 549 cm<sup>-1</sup> corresponding to the Fe-O. In the same way, the functionalization of nanoparticles with APTMS was highlighted for **Fe<sub>3</sub>O<sub>4</sub>-PABA-SiO<sub>2</sub>-4**.

The magnetic properties of **Fe<sub>3</sub>O<sub>4</sub>-PABA-SiO<sub>2</sub>-4-APS** nanoparticles were measured using a vibrating sample magnetometer (VSM) obtaining a value of saturation magnetization Ms= 50.883 emu/g. The nanoparticles obtained by this method were also efficiently separated by an external magnetic field.

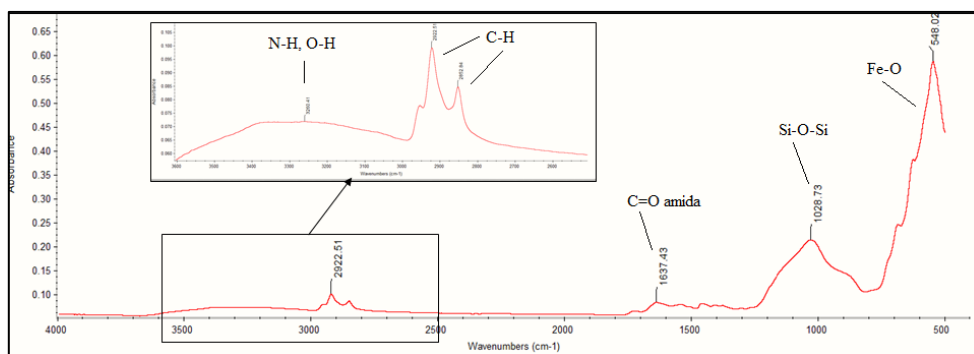


Figure 5.50. FT-IR spectrum for **Fe<sub>3</sub>O<sub>4</sub>-PABA-SiO<sub>2</sub>-3-APS-HMBA**

Obtaining the **Fe<sub>3</sub>O<sub>4</sub>-PABA-SiO<sub>2</sub>-3-APS-HMBA** nanostructured system by attaching the HMBA linker to the APTMS-functionalized silica shell was confirmed by the FT-IR spectrum by the presence of the C=O stretching vibration of the secondary amide newly formed by attaching the 1637 cm<sup>-1</sup> linker. Also, can be observed the bands characteristic of the N-H and O-H stretching vibrations at 3260 cm<sup>-1</sup>, the band corresponding to the C-H stretching vibration at 2922 and 2852 cm<sup>-1</sup>. Also highlighted are the bands characteristic of the inorganic support, the asymmetric stretching vibration of Si-O-Si at 1028 cm<sup>-1</sup> and 548 cm<sup>-1</sup> and respectively the band characteristic of magnetite corresponding to the Fe-O bond. In the same

way, the success of obtaining the **Fe<sub>3</sub>O<sub>4</sub>-PABA-SiO<sub>2</sub>-4-APS-HMBA** nanostructured system was highlighted.

### 5.2.3.3. Obtaining and characterization of the **Fe<sub>3</sub>O<sub>4</sub>-PABA-SiO<sub>2</sub>-SiLOH** nanostructured system

The **Fe<sub>3</sub>O<sub>4</sub>-PABA-SiO<sub>2</sub>-SiL-OH** nanostructured system (Fig. 5.52) was synthesized based on **Fe<sub>3</sub>O<sub>4</sub>-PABA-SiO<sub>2</sub>-1** core-shell nanoparticles.

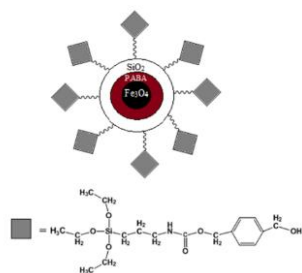
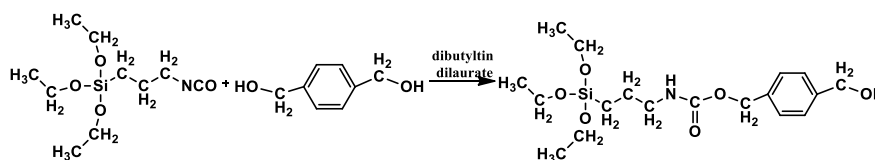


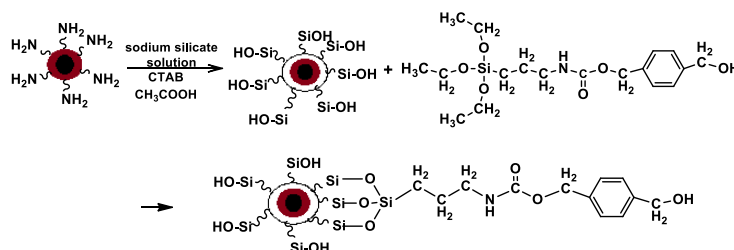
Figure 5.52. Graphical representation of **Fe<sub>3</sub>O<sub>4</sub>-PABA-SiO<sub>2</sub>-SiL-OH** nanostructured system

An organic linker system, SiL-OH, similar to the linker commonly used in SPPS, namely HMBA, was obtained from 1,4-dimethylolbenzene and *gamma*-isocyanatopropyltriethoxysilane (Scheme 5.10) and was subsequently grafted onto the surface of the nanoparticles **Fe<sub>3</sub>O<sub>4</sub>-PABA-SiO<sub>2</sub>-1** according to the series of reactions shown in Scheme 5.11.



Scheme 5.10. Synthesis of the **SiL-OH** linker system

The selected linker system contains a  $-CH_2-OH$  terminal group in the benzyl position, providing a reversible link between the peptide chain and the solid support, thus ensuring the protection and blocking of the C-terminus during the solid phase peptide synthesis process [138].



Scheme 5.11. Synthesis of the **Fe<sub>3</sub>O<sub>4</sub>-PABA-SiO<sub>2</sub>-SiL-OH** nanostructured system

The structure of the **SiL-OH** linker system was confirmed by <sup>1</sup>H NMR, <sup>13</sup>C NMR and FT-IR by identifying specific chemical shifts and by the presence of absorption bands



characteristic. Signal attributions in the proton and carbon NMR spectra of the system **SiL-OH** are shown in Figure 5.53.

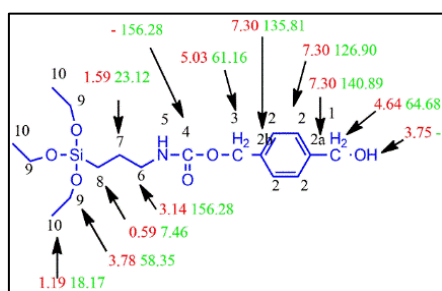


Figure 5.53. Chemical shifts,  $\delta^1\text{H}$  and  $\delta^{13}\text{C}$  of **SiL-OH**

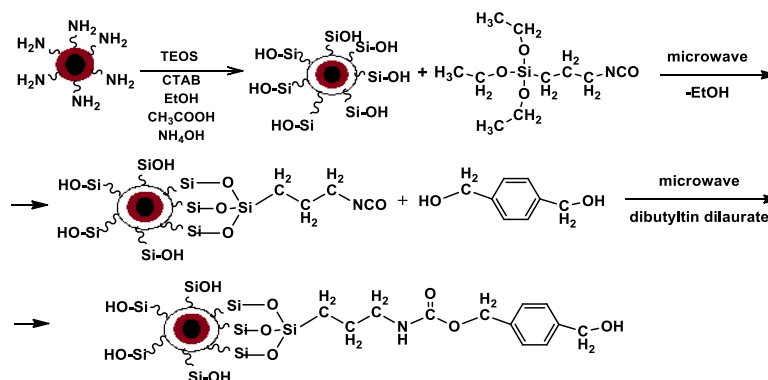
The structure of **SiL-OH** linker system obtained, was also confirmed by FT-IR by the presence of characteristic absorption bands stretching vibration N-H<sub>urethane</sub> at 3331  $\text{cm}^{-1}$  and C=O<sub>urethane</sub> at 1695  $\text{cm}^{-1}$ . The band corresponding to the N-H deformation vibration can be observed at 1528  $\text{cm}^{-1}$  and the band corresponding to the stretching vibration N-CO-O at 1244  $\text{cm}^{-1}$ . The aromatic structure is highlighted by the presence of characteristic bands C<sub>Ar-H</sub> at 769  $\text{cm}^{-1}$ . The band corresponding to the asymmetric stretching vibrations Si-O-Si can be observed at 1072  $\text{cm}^{-1}$  and the band corresponding to the stretching vibration C-H at 2926  $\text{cm}^{-1}$ .

Obtaining the **Fe<sub>3</sub>O<sub>4</sub>-PABA-SiO<sub>2</sub>-SiL-OH** nanostructured system was demonstrated by the FTIR spectrum by the presence of deformation bands for the secondary amine at 1519  $\text{cm}^{-1}$ , stretching bands C=O at 1692  $\text{cm}^{-1}$  and N-H at 3331  $\text{cm}^{-1}$  and characteristic bands C-H stretching vibration at 2927  $\text{cm}^{-1}$  as well as the corresponding deformation vibrations aromatic structure C<sub>Ar-H</sub> at 772  $\text{cm}^{-1}$  which confirms the presence of aliphatic and aromatic units related to core-shell-silica nanoparticles. The presence of the silica coating is confirmed by the band corresponding to the asymmetric vibration Si-O-Si at 1000  $\text{cm}^{-1}$ , and at 550  $\text{cm}^{-1}$  the characteristic band of magnetite corresponding to the Fe-O bond.

#### 5.2.3.4. Obtaining and characterization of the **Fe<sub>3</sub>O<sub>4</sub>-PABA-SiO<sub>2</sub>-SiL-OH<sub>mw</sub>** nanostructured system

Given the agglomeration trend observed in TEM micrographs for **Fe<sub>3</sub>O<sub>4</sub>-PABA-SiO<sub>2</sub>** systems for which the CTAB template was removed by calcination affecting the specific surface of the nanoparticles, and therefore also the expected performance in SPPS a new strategy was addressed approached for the synthesis of a nanostructured linker system **SiL-OH** by using a raw material that is not calcined, namely **Fe<sub>3</sub>O<sub>4</sub>-PABA-SiO<sub>2</sub>-2**. Working procedure adopted for the final nanostructured system **Fe<sub>3</sub>O<sub>4</sub>-PABA-SiO<sub>2</sub>-SiL-OH<sub>mw</sub>** was the sequential functionalization of **Fe<sub>3</sub>O<sub>4</sub>-PABA-SiO<sub>2</sub>-2** nanoparticles, with *gamma*-

isocyanatopropyltriethoxysilane and 1,4-dimethylolbenzene using the microwave irradiation in the presence of dibutyltin dilaurate as shown in Scheme 5.12 [138].



Scheme 5.12. Synthesis of the  $\text{Fe}_3\text{O}_4\text{-PABA-SiO}_2\text{-SiL-OHmw}$  nanostructured system

Obtaining the  $\text{Fe}_3\text{O}_4\text{-PABA-SiO}_2\text{-SiL-OHmw}$  nanostructured system was demonstrated by the FT-IR spectrum by the presence of deformation for amine secondary to  $1538\text{ cm}^{-1}$ , stretching bands  $\text{C}=\text{O}$  at  $1694\text{ cm}^{-1}$  for amide and  $\text{N-H}$  bond at  $3325\text{ cm}^{-1}$  and the bands characteristic of the  $\text{C-H}$  stretching vibration at  $2926\text{ cm}^{-1}$  and deformation vibrations corresponding to the aromatic structure  $\text{C}_{\text{Ar-H}}$  at  $775\text{ cm}^{-1}$  which confirms the presence of aliphatic and aromatic units related to core-shell-silica nanoparticles. The presence of the silica coating is confirmed by the band corresponding to the asymmetric  $\text{Si-O-Si}$  vibration at  $1015\text{ cm}^{-1}$ .

### 5.3. Conclusions

The  $\text{Fe}_3\text{O}_4\text{-PABA}$  core-shell magnetic nanoparticles were synthesized by the coprecipitation method and the silica secondary shell was obtained by a modified sol-gel method using a sodium silicate solution ( $\rho=1.39\text{ g mL}^{-1}$ ) and TEOS as sources of silica.

The bioavailability of  $\text{Fe}_3\text{O}_4\text{-PABA}$  magnetic nanoparticles was determined using the chicken embryo chorioallantoic membrane (CAM) model and the murine model.

Four new types of nanostructured systems based on organic nanoparticles with organic shell (PABA) and silica secondary shell to form a solid support have been designed for solid phase peptide synthesis:  $\text{Fe}_3\text{O}_4\text{-PABA-GA-PPD}$ ,  $\text{Fe}_3\text{O}_4\text{-PABA-SiO}_2\text{-APS-HMBA}$ ,  $\text{Fe}_3\text{O}_4\text{-PABA-SiO}_2\text{-SiL-OH}$  and  $\text{Fe}_3\text{O}_4\text{-PABA-SiO}_2\text{-SiL-OHw}$ . These systems are decorated with linkers similar to those frequently used in the synthesis of solid phase peptides. A new SiL-OH linker system with free  $-\text{CH}_2\text{-OH}$  group was obtained from *gamma*-isocyanatopropyltriethoxysilane and 1,4-dimethylolbenzene.

All types of synthesized nanoparticles and nanostructured systems with applications in solid phase synthesis were characterized using modern methods of investigation: XRD, FT-IR, TEM, SEM, EDX, DLS, BET, VSM.

## CHAPTER 6. ORIGINAL CONTRIBUTIONS TO THE ELECTRONIC APPLICATIONS OF $\text{Fe}_3\text{O}_4$ -PABA NANOPARTICLES AND THE INVESTIGATION OF THE ELECTRICAL PROPERTIES OF $\text{Fe}_3\text{O}_4$ -PABA- $\text{SiO}_2$ NANOFILM DOPED WITH DPPH RADICAL

The following objectives have been considered in this chapter:

- (a) Special applications of  $\text{Fe}_3\text{O}_4$ -PABA nanoparticles: Obtaining the transistor based on  $\text{Fe}_3\text{O}_4$ -PABA nanoparticles
- (b) Investigation of the electrical properties of  $\text{Fe}_3\text{O}_4$ -PABA- $\text{SiO}_2$  nanofilm doped with DPPH radical

### 6.1. Special applications of $\text{Fe}_3\text{O}_4$ -PABA nanoparticles: Obtaining the transistor based on $\text{Fe}_3\text{O}_4$ -PABA nanoparticles

Nanoparticle-based transistor  **$\text{Fe}_3\text{O}_4$ -PABA** it functioned as an electronic device by placing two thin probes on top of the  **$\text{Fe}_3\text{O}_4$ -PABA** film, as Source and Drain contacts. The ITO electrode was used as the Gate electrode. Three  **$\text{Fe}_3\text{O}_4$ -PABA** films with different thicknesses of each layer, namely: 200, 400 and 600 nm were deposited on the same substrate previously coated with a 100 nm polystyrene layer, by the Dip Coating method [137].

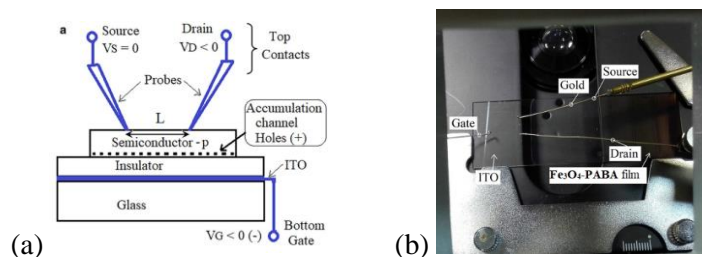


Figure 6.1. (a) Organic thin film transistors (OTFT) test structure, similar to the bottom gate top contacts (BGTC) p-type transistor [181] (b) testing the electrical properties of the nanoparticle-based transistor  **$\text{Fe}_3\text{O}_4$ -PABA**

The output characteristics emphasises a quasi-linear region, followed by a saturation region that is specific to a p-film OTFT (Fig. 6.2.a).

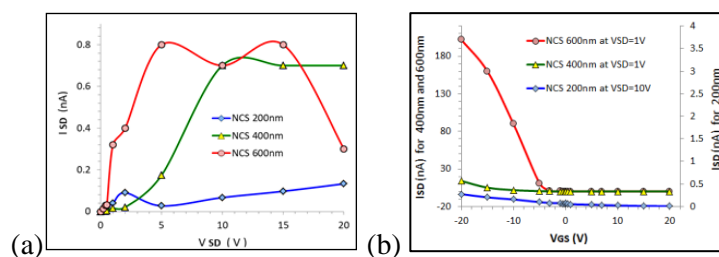
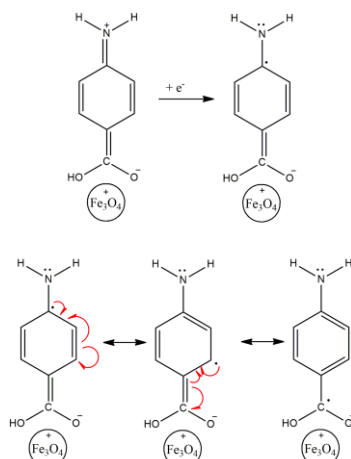


Figure 6.2. The measured curves family of the organic transistor  **$\text{Fe}_3\text{O}_4$ -PABA** fabricated: (a) output characteristics at  $V_{GS}=0$  V; (b) transfer characteristics at different  $V_{SD}$ : 1 V for 200, 400 and 600 nm thicknesses, respectively, and 10 V only for 200 nm thickness

The behavior of the  **$\text{Fe}_3\text{O}_4$ -PABA** film as a p-type was attributed to the ability of the organic compound, PABA, to function as an electron acceptor, by obtaining a cationic radical

system as a result of the transfer of an electron, a system stabilized by conjugation capable of yielding in turn the electron by returning to the structure initial, according to Scheme 6.1.



Scheme 6.1. Stabilization as a radical-cation by acceptance of 1 electron for the **Fe<sub>3</sub>O<sub>4</sub>-PABA** nanostructured system

Accumulation at negative gate voltages (Fig. 6.2.b) is the most efficient regime. This is the main proof that the **Fe<sub>3</sub>O<sub>4</sub>-PABA** film shows a „p” type behavior for the fabricated OTFT [137].

## 6.2. Investigation of the electrical properties of *Fe<sub>3</sub>O<sub>4</sub>-PABA-SiO<sub>2</sub>* nanofilm doped with DPPH radical

Highly polarizable organic compounds, such as rich or electron-deficient species (eg diphenyl-picryl-hydrazyl radical, phenylsidone or polyaniline) are good candidates for electron transfer applications in electronics, such as: TFT transistor (thin film transistor).

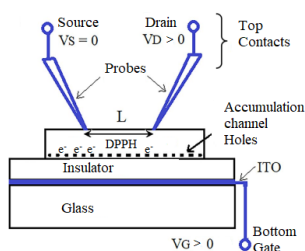
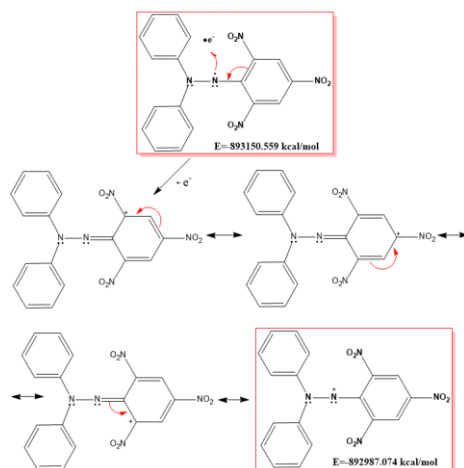


Figure 6.5. Organic thin-film (TFT) transistor test structure with field-effect transistor behavior

The „n” type character of **Fe<sub>3</sub>O<sub>4</sub>-PABA-SiO<sub>2</sub> nanofilm doped with DPPH radical** was proved by static measurements. Behavior as an „n” type semiconductor a **Fe<sub>3</sub>O<sub>4</sub>-PABA-SiO<sub>2</sub> nanofilm doped with DPPH radical** was attributed to the ability of the DPPH radical to function as an electron donor, by obtaining a cationic system following the transfer of an electron, a system stabilized by conjugation, capable of accepting the electron in turn by returning to the original structure, according to Scheme 6.2.



Scheme 6.2. Limit structures of DPPH<sup>+</sup> carbocation formed by 1 electron transfer

The Gamess molecular modelling program was used to optimize the theoretical structure of the DPPH radical and the structure resulting from the transfer of 1 electron, as well as to highlight the partial charge distribution of these two structures. It is found, as demonstrated by the boundary structures, a stabilization of them by conjugation on the aromatic system. The energy difference ( $\Delta E = -163.485$  Kcal/mol) theoretically justifies the semiconductor behavior of the DPPH radical by 1 electron transfer.

### 6.2.1. Characterization of Fe<sub>3</sub>O<sub>4</sub>-PABA-SiO<sub>2</sub> nanofilm doped with DPPH radical

In the mass spectrum (Fig. 6.9) obtained using the ESI ionization technique and the introduction of the sample by direct infusion, the molecular ion corresponding to the DPPH radical [*m/z* 394] can be observed as well as the specific isotopic distribution [*M*+1] and [*M*+2].

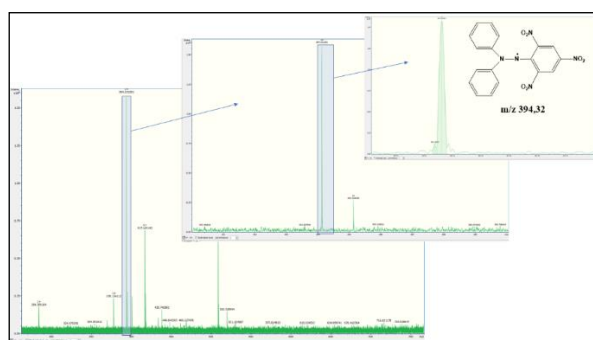


Figure 6.9. HR-MS analysis of the DPPH radical solution

Confirmation of the molecular peak in MALDI analyses (Fig. 6.10) shows the successful and without degradation transfer of the radical system in the nanostructured matrix and then in the thin film. The MALDI ionization method was used based on the protection characteristic of the analysed compound by transferring energy from the matrix to the sample during the laser ablation process. Given the use of magnetic nanoparticles as a matrix for MALDI analyses for the analysis of small mass molecules [186] it was not necessary to use an

additional matrix because the intrinsic ionization produced by the **Fe<sub>3</sub>O<sub>4</sub>-PABA-SiO<sub>2</sub>-4** nanoparticles it was enough.

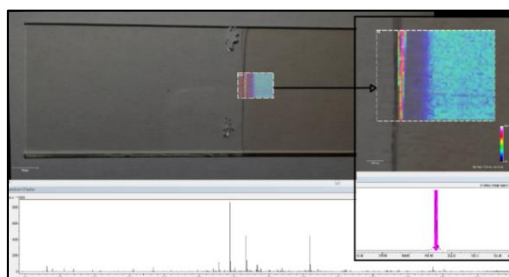


Figure 6.10. MALDI analysis of **Fe<sub>3</sub>O<sub>4</sub>-PABA-SiO<sub>2</sub> nanofilm doped with DPPH radical**

#### *Homogeneity estimation of **Fe<sub>3</sub>O<sub>4</sub>-PABA-SiO<sub>2</sub> nanofilm doped with DPPH radical***

The homogeneity of the film deposition was highlighted by the homogeneity of the spectral response (Fig. 6.10. And 6.11.) Using the following characterization techniques: MALDI and FT-IR microscopy. For the obtained nanofilm, a discontinuity zone in the starting zone is also observed.

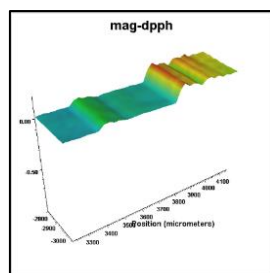


Figure 6.11. FT-IR microscopy analysis of **Fe<sub>3</sub>O<sub>4</sub>-PABA-SiO<sub>2</sub> nanofilm doped with DPPH radical**

The „n” type character of **Fe<sub>3</sub>O<sub>4</sub>-PABA-SiO<sub>2</sub> nanofilm doped with DPPH radical** was proved by static measurements.

### **6.3. Conclusions**

The electrical properties of nanofilms **Fe<sub>3</sub>O<sub>4</sub>-PABA** and **Fe<sub>3</sub>O<sub>4</sub>-PABA-SiO<sub>2</sub> doped with DPPH radical** obtained by the Dip-Coating method was investigated.

The **Fe<sub>3</sub>O<sub>4</sub>-PABA** nanofilm obtained functioned as an electronic device with a "p" type behavior for the OTFT (organic thin film transistor) model fabricated.

The **Fe<sub>3</sub>O<sub>4</sub>-PABA-SiO<sub>2</sub> nanofilm doped with DPPH radical** obtained functioned as an electronic device with a TFT type transistor behavior (thin film transistor) with n-type film. The „n” type character of **Fe<sub>3</sub>O<sub>4</sub>-PABA-SiO<sub>2</sub> nanofilm doped with DPPH radical** was proved by measurements of the static characteristics of the device.

## CHAPTER 7. ORIGINAL CONTRIBUTIONS ON PEPTIDE SYNTHESIS ON MAGNETIC NANOSTRUCTURED SUPPORT (NSS)

This chapter presents the testing of new synthesized nanostructured systems as a solid support for solid support peptide synthesis. The working protocol involved „Fmoc synthesis strategy”.

### 7.1 Objectives of experimental research

- (1) Synthesis of peptides on magnetic nanostructured support
- (2) Characterization and identification of the peptide fragments obtained

### 7.2 Synthesis of peptides on magnetic nanostructured support

The solid phase peptide synthesis method on a magnetically nanostructured solid support called Synthesis on Nanostructured Support (NSS) was used to overcome the problem of solubility, giving the advantage of the access of the reactants to the reaction center; but also a rapid separation of intermediate and final products from the reaction medium in the magnetic field. The efficiency of the new synthesized nanostructured systems has been demonstrated by using them as a solid support in peptide synthesis according to Table 7.2. using the SPPS principle.

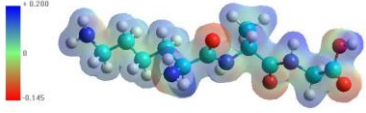
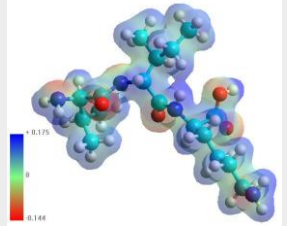
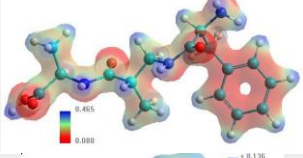
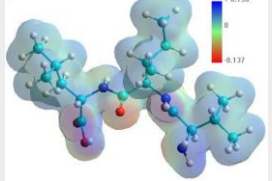
Table 7.2. Peptide sequences obtained by NSS strategy

<i>Magnetic nanostructured support</i>	<i>Peptide sequence</i>	<i>m/z theoretical</i>	<i>m/z experimental</i>	<i>Characterization method</i>
<b>Fe<sub>3</sub>O<sub>4</sub>-PABA-GA-PPD</b>	<b>Lys-Ala-Gly</b>	275.17	275.08	LC-MS
<b>Fe<sub>3</sub>O<sub>4</sub>-PABA-SiO<sub>2</sub>-APS-HMBA</b>	<b>Val-Ile-Lys</b>	359.26	359.34	HR-MS
<b>Fe<sub>3</sub>O<sub>4</sub>-PABA-SiO<sub>2</sub>-SiL-OH</b>	<b>Gly-Ala-Phe</b>	359.34	294.20	LC-MS
<b>Fe<sub>3</sub>O<sub>4</sub>-PABA-SiO<sub>2</sub>-SiL-OHmw</b>	<b>Leu-Ile-Val</b>	344.25	344.22	LC-MS

The selection criteria of the amino acids used in the synthesis of peptides were aimed at obtaining peptides of biological importance that are found in peptides found in nature or that have important biological / pharmacological properties. Also, to determine the limits between which this solid phase synthesis method can be used, branched side chain amino acids were used, as well as other functional groups that require additional protection / deprotection operations. The influence of steric hindrance on the performance of the solid phase synthesis method on the different types of newly synthesized solid support was estimated by the use of amino acids with different side chain volumes. Information on the volume and spatial structure of the synthesized peptides was obtained using the Hyperchem 8.0 molecular modelling

program. The amino acids used were glycine, alanine, lysine, phenylalanine, valine, leucine, isoleucine.

Table 7.3. Information on the volume and spatial structure of the synthesized peptides obtained using the Hyperchem 8.0 molecular modelling program

<i>Peptide sequence</i>	<i>Structure of the optimized peptide sequence in Hyperchem 8.0</i>
Lys-Ala-Gly (KAG)	
Val-Ile-Lys (VIK)	
Gly-Ala-Phe (GAF)	
Leu-Ile-Val (LIV)	

The experimental results obtained by FT-MS (Table 7.2.) Show the successful obtaining of the proposed peptide sequences; as well as the feasibility of the peptide synthesis method using as a solid support a magnetic nanostructured system through the Fmoc synthesis strategy.

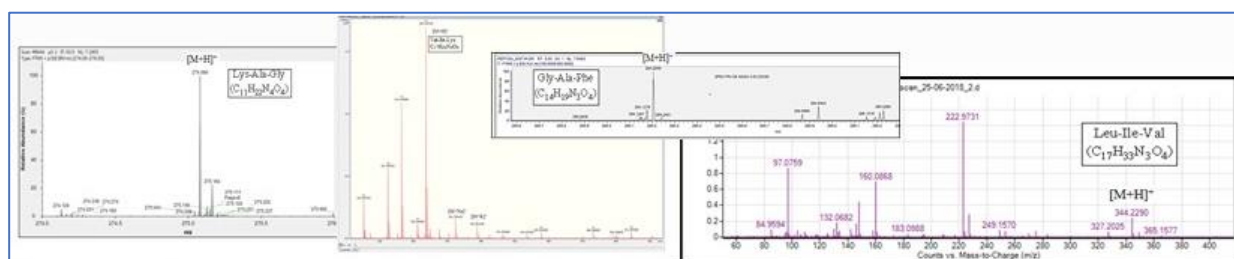


Figure 7.21. FT-MS analysis for synthesized peptides

### 7.2.2 Obtaining and characterizing of Val-Ile-Lys peptide

Peptide sequence Val-Ile-Lys was synthesized using as a solid support the **Fe<sub>3</sub>O<sub>4</sub>-PABA-SiO<sub>2</sub>-3-APS-HMBA** nanostructured system, as well as the **Fe<sub>3</sub>O<sub>4</sub>-PABA-SiO<sub>2</sub>-4-APS-HMBA** nanostructured system.



In the mass spectrum (Fig. 7.22.) Obtained by HR-MS using the ESI ionization technique and the introduction of the sample by direct infusion, the protonated molecular ion  $[M+H]^+$  at  $m/z$  359.34 can be observed according to the values calculated using software available online PROTEOMICS TOOLKIT. Also, the peaks at  $m/z$  381,32 corresponding to  $[M+Na]^+$  and  $m/z$  397.30 corresponding to  $[M+K]^+$ . Isotopic peaks of type  $([M+H]^+ + 1)$ ,  $([M+H]^+ + 2)$ ,  $([M+H]^+ + 3)$  derives from the protonated molecular ion  $[M+H]^+$ . As a result, they will be at 2, 3, 4 u.a.m difference from the molecular ion.

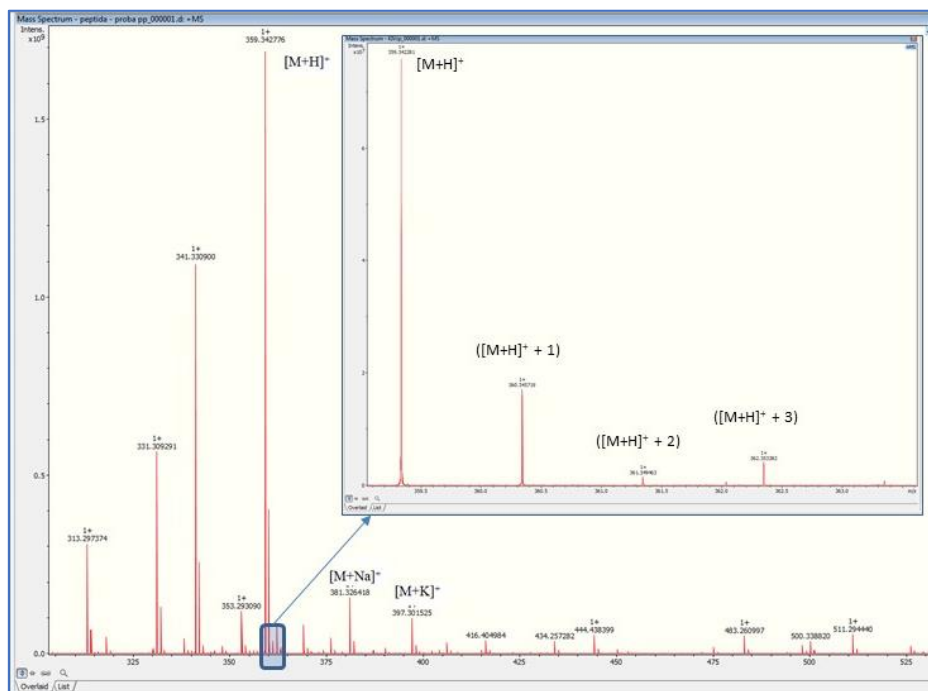


Figure 7.22. HR-MS analysis of the peptide **Val-Ile-Lys**

### 7.3. Identification of peptides and possible fragments obtained by FT-MS analysis

Mass spectrometry is used for the analysis of peptides and proteins due to its speed, sensitivity and versatility. It can be used to determine the amino acid sequences of peptides, but also to characterize a wide variety of posttranslational changes, such as phosphorylation and glycosylation [193].

During ionization, protonation occurs at basic sites, and the different protonated forms of a peptide or protein depend on both the internal energy of the ions and the basicity of the positions involved in the protonation process. The presence of a task at a particular site may favor the fragmentation of adjacent links [194]. Fragments can only be detected if they have at least one load. If the charge is at the N-terminus, the ions are called a, b or c. If the charge is at the C-terminus, the ions are called x, y or z [193].

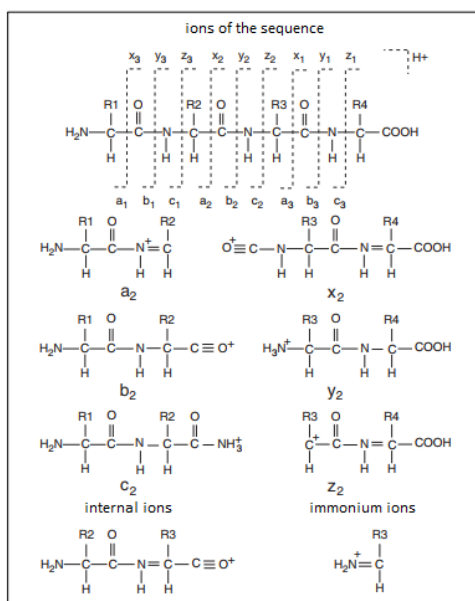


Figure 7.16. Nomenclature for ions of peptide fragments resulting from fragmentation reactions (R - amino acid side chain) [193]

### 7.3.2. Identification of Val-Ile-Lys and possible fragments

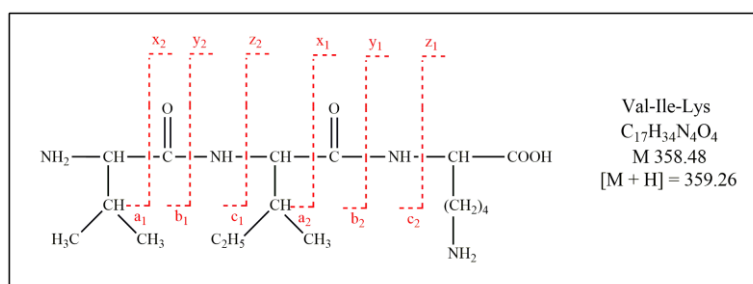
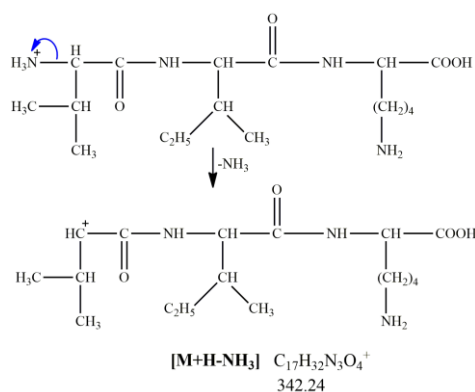


Figure 7.18. The types of fragments that can be obtained for the **Val-Ile-Lys** peptide

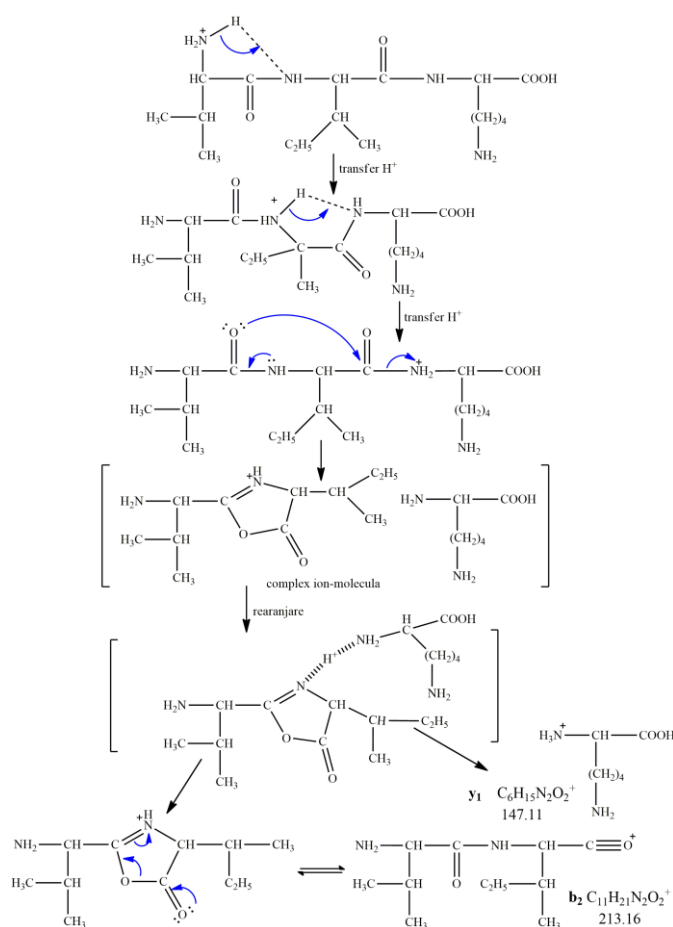
Possible mechanisms of formation of fragments of type  $[\text{M} + \text{H} - \text{NH}_3]^+$ ,  $b_1$ ,  $b_2$ ,  $y_1$ ,  $a_1$ ,  $a_2$ ,  $y_1 - \text{NH}_3$ ,  $y_2 - \text{NH}_3$  can be observed in Schema 7.8, Schema 7.9, Schema 7.10., Schema 7.11 (Schema 7.9, Schema 7.10. adapted according to ref. [197]; Schema 7.11. adapted according to ref. [199]):



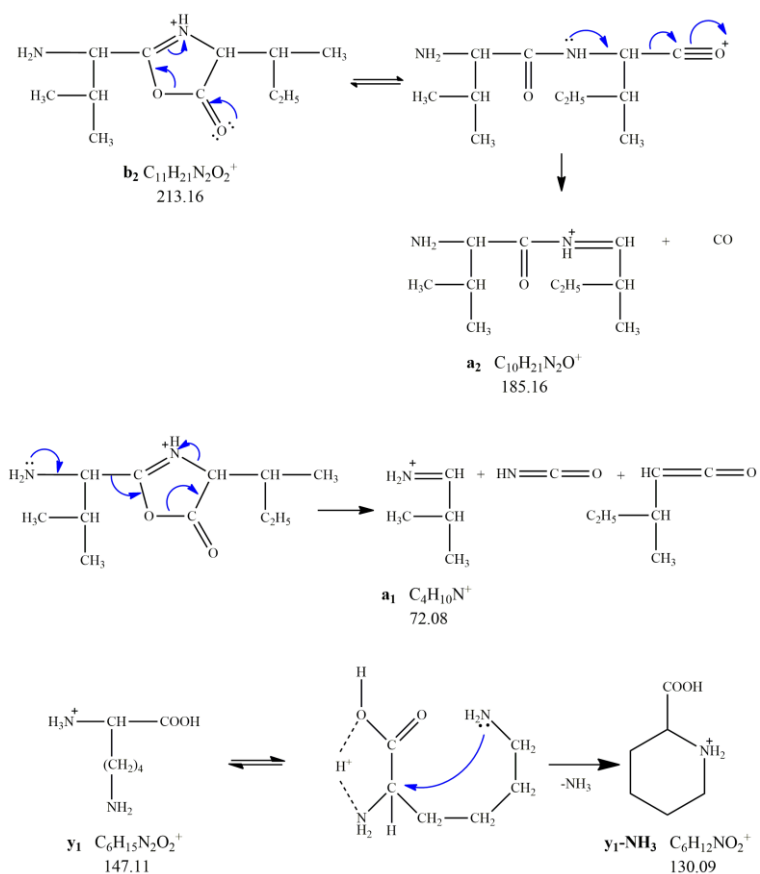
Scheme 7.8. Possible mechanism of fragment formation  $[\text{M} + \text{H} - \text{NH}_3]^+$

The use of collision-induced dissociation for precursor ions leads to rupture of the amide bonds of protonated peptides, leading to the formation of mainly y type and b type ions. This behavior is initiated by the transfer of proton to the nitrogen atom involved in the amide bond, which leads to the weakening of the peptide bonds and their rupture with the formation of the corresponding fragments. Therefore, such a proton transfer involves the existence of a "mobile" proton, and the carbon atom involved in the amide bond may undergo a nucleophilic attack to form by cyclization the corresponding oxazolone into the protonated form and the subsequent release of the C-terminal fragment of the peptide.

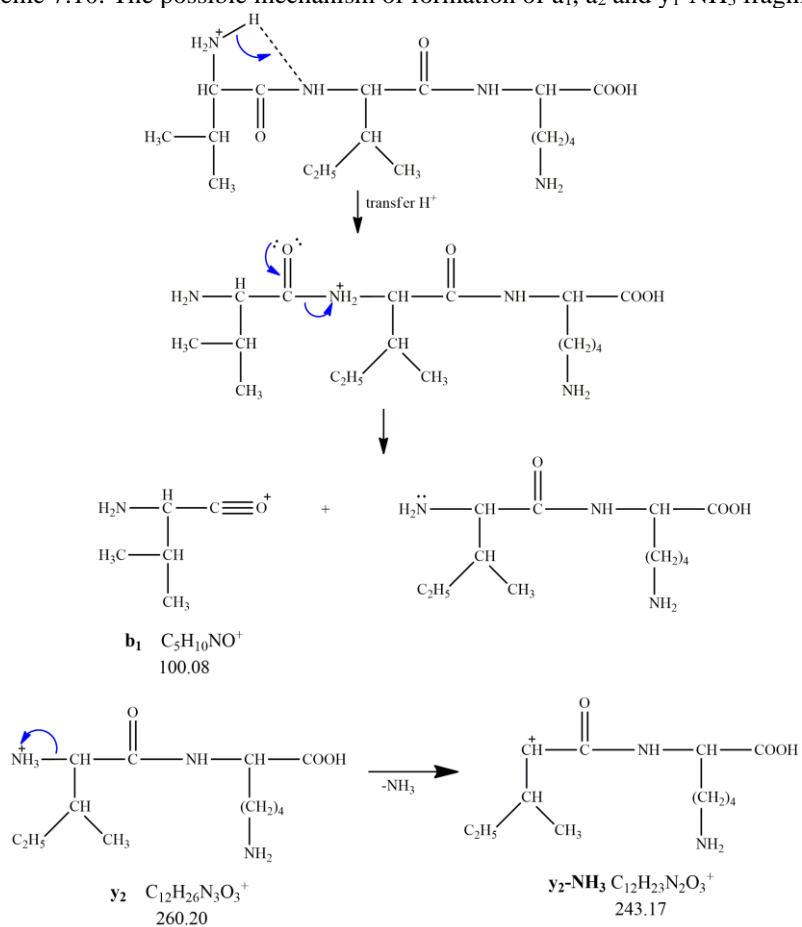
As can be seen in the mechanism proposed in Scheme 7.9., The N-terminal and C-terminal fragment of the exemplified peptide can be attached by non-covalent association to form an ion-dipole complex, which undergoes rearrangement by forming a proton-bound dimer, which can competitively lead to the formation of an y type ion or b type ion, depending on the relative affinity of the proton; fragments that may undergo further fragmentation as can be seen in Scheme 7.10 [197].



Scheme 7.9. The possible mechanism of formation of b<sub>2</sub> and y<sub>1</sub> fragments



Scheme 7.10. The possible mechanism of formation of  $\text{a}_1$ ,  $\text{a}_2$  and  $\text{y}_1\text{-NH}_3$  fragments



Scheme 7.11. The possible mechanism of formation of  $\text{b}_1$  and  $\text{y}_2\text{-NH}_3$  fragments

Table 7.6. Other types of fragments corresponding to the **Val-Ile-Lys** peptide

<i>Fragment type</i>	<i>Chemical formula</i>	<i>m/z theoretical</i>	<i>m/z experimental</i>
<b>[M+H-H<sub>2</sub>O]<sup>+</sup></b>	C <sub>17</sub> H <sub>33</sub> N <sub>4</sub> O <sub>3</sub> <sup>+</sup>	341.25	341.26
<b>[M+H-CO-H<sub>2</sub>O]<sup>+</sup></b>	C <sub>16</sub> H <sub>33</sub> N <sub>4</sub> O <sub>2</sub> <sup>+</sup>	313.26	313.22
<b>[M+H-NH<sub>3</sub>]<sup>+</sup></b>	C <sub>17</sub> H <sub>32</sub> N <sub>3</sub> O <sub>4</sub> <sup>+</sup>	342.23	342.26
<b>[M-H<sub>2</sub>O+Na]<sup>+</sup></b>	C <sub>17</sub> H <sub>32</sub> N <sub>4</sub> O <sub>3</sub> Na <sup>+</sup>	363.23	363.30
<b>[M+H-2H<sub>2</sub>O]<sup>+</sup></b>	C <sub>17</sub> H <sub>31</sub> N <sub>4</sub> O <sub>2</sub> <sup>+</sup>	323.24	323.24

The following types of fragments corresponding to the peptide were identified in the MS-MS spectra (ANNEX 2) **Val-Ile-Lys**: c<sub>1</sub>, y<sub>1</sub>, z<sub>1</sub> with m/z 117.43, 130.16, respectively 147.99 (Fig. A2.7.); x<sub>1</sub> and a<sub>2</sub> cu m/z 173.00, respectively 185.92 (Fig. A2.8.); b<sub>2</sub>, c<sub>2</sub> and z<sub>2</sub> with m/z 213.90, 230.99, respectively 243.80 (Fig. A2.9.); x<sub>2</sub> and y<sub>2</sub> with m/z 286.82 and 260.88 (Fig. A2.10.) and [M+H-H<sub>2</sub>O]<sup>+</sup>, [M+H-CO-H<sub>2</sub>O]<sup>+</sup>, [M+H-NH<sub>3</sub>]<sup>+</sup>, [M-H<sub>2</sub>O+Na]<sup>+</sup>, [M+H-2H<sub>2</sub>O]<sup>+</sup> with m/z 341.26, 313.22, 342.26, 363.30, respectively 323.24 ( Fig. A2.11.).

#### 7.4. Conclusions

Synthesized nanostructured systems: **Fe<sub>3</sub>O<sub>4</sub>-PABA-GA-PPD**, **Fe<sub>3</sub>O<sub>4</sub>-PABA-SiO<sub>2</sub>-APS-HMBA**, **Fe<sub>3</sub>O<sub>4</sub>-PABA-SiO<sub>2</sub>-SiL-OH** and **Fe<sub>3</sub>O<sub>4</sub>-PABA-SiO<sub>2</sub>-SiL-OH** were tested by successfully coupling three different Fmoc-protected amino acids. The different morphologies of the silica secondary shell influence the dispersibility of nanostructured systems in solvents used in solid phase synthesis, but do not affect the performance of the presented peptide synthesis.

The experimental results obtained by FT-MS show the successful obtaining of the proposed peptide sequences (**Lys-Ala-Gly**, **Val-Ile-Lys**, **Gly-Ala-Phe** and **Lys-Ile-Val**), as well as the feasibility of the peptide synthesis method using as a solid support a magnetic nanostructured system through the Fmoc synthesis strategy.

## CHAPTER 8. GENERAL CONCLUSIONS

Solid phase peptide synthesis is one of the main methods of peptide synthesis. SPPS performance depends largely on the type of solid support used and can be improved by using magnetic nanoparticles as a solid support instead of the conventional polymeric support offering the advantage of obtaining a high specific surface, the magnetic properties of the magnetic core allowing quick and easy extraction of the product from the reaction mixture. Also, the accessibility to the surface functionalities is improved by the direct access to the reaction center, and the magnetic sedimentation facilitates the whole intermediate washing operation, thus allowing a better management of the reactants.

The research objective of this doctoral thesis was focused on the development of a new SPPS approach, namely the synthesis of peptides on magnetic nanostructured support. To this end, instead of the standard solid support, consisting of a functionalized resin, we have developed new types of solid support consisting of core-shell ferrite nanoparticles with PABA, silica secondary shell and various linker systems with polar terminal grouping, labile under final cleavage conditions, capable of efficiently binding N-terminal blocked amino acids and compatible with all stages of said peptide synthesis. The ability to attach new nanostructured systems using the SPPS principle was tested by successively coupling three different Fmoc-protected amino acids.

The **Fe<sub>3</sub>O<sub>4</sub>-PABA** core-shell magnetic nanoparticles were synthesized by the coprecipitation method. The crystal structure of **Fe<sub>3</sub>O<sub>4</sub>-PABA** nanoparticles was demonstrated by XRD and SAED analysis; and their size and morphology through DLS, TEM and SEM. The presence of the PABA shell was confirmed by FT-IR. The specific surface area was estimated by BET analysis and the magnetic properties were measured using a vibrating sample magnetometer (VSM). Bioavailability of **Fe<sub>3</sub>O<sub>4</sub>-PABA** nanoparticles was determined using the chicken embryo chorioallantoic membrane (CAM) model and the murine model. PABA shell on the surface of Fe<sub>3</sub>O<sub>4</sub> nanoparticles allows persistence in circulation and easy handling under the action of a static magnetic field of the ferromagnetic nanoparticles it functions. Nanoparticles of the type **Fe<sub>3</sub>O<sub>4</sub>-PABA** are biocompatible and have a low risk of intravenous embolism.

The secondary silica shell was obtained by a modified sol-gel method using a sodium silicate solution ( $\rho=1.39 \text{ g mL}^{-1}$ ) and TEOS as sources of silica. A comparative study was performed to remove the template by calcination, respectively, washing with solvents. Washing with EtOH / 5% acetic acid followed by washing with EtOH allowed an efficient removal of

template. Structure and morphology of the obtained **Fe<sub>3</sub>O<sub>4</sub>-PABA-SiO<sub>2</sub>** magnetic nanoparticles was investigated using advanced analysis techniques, namely: XRD, SEM, TEM, EDX, FTIR. In order to establish the heat treatment regime, the TGA analysis was performed, and the specific surface of the obtained material was estimated by BET analysis. The magnetic properties were measured using a vibrating sample magnetometer (VSM).

Four new types of nanostructured systems based on organic nanoparticles with organic shell (PABA) and silica secondary shell to form a solid support have been designed for solid phase peptide synthesis: **Fe<sub>3</sub>O<sub>4</sub>-PABA-GA-PPD**, **Fe<sub>3</sub>O<sub>4</sub>-PABA-SiO<sub>2</sub>-APS-HMBA**, **Fe<sub>3</sub>O<sub>4</sub>-PABA-SiO<sub>2</sub>-SiL-OH** and **Fe<sub>3</sub>O<sub>4</sub>-PABA-SiO<sub>2</sub>-SiL-OHmw**.

The **Fe<sub>3</sub>O<sub>4</sub>-PABA-GA-PPD** magnetic nanostructured system designed to be used as a solid support for peptide synthesis was obtained using magnetic nanoparticles of the type core-shell, **Fe<sub>3</sub>O<sub>4</sub>-PABA** and an ambident linker system with grouping -NH<sub>2</sub> free, compatible with all stages of synthesis. Glutaraldehyde (GA) was used as a linker to obtain a group -NH<sub>2</sub> reactive at the end of the linker system, capable of efficiently binding N-terminally blocked amino acids, grafted *p*-phenylenediamine (PPD). The presence of glutaraldehyde grafted on the **Fe<sub>3</sub>O<sub>4</sub>-PABA** surface nanoparticles and subsequent attachment of *p*-phenylenediamine was confirmed by FT-IR spectrometry.

The new magnetic nanostructured system, **Fe<sub>3</sub>O<sub>4</sub>-PABA-SiO<sub>2</sub>-APS-HMBA** designed to be used as a solid support in SPPS was obtained by coating the surface of nanoparticles magnetic with silica secondary shell (**Fe<sub>3</sub>O<sub>4</sub>-PABA-SiO<sub>2</sub>-3** and **Fe<sub>3</sub>O<sub>4</sub>-PABA-SiO<sub>2</sub>-4**) with 3-aminopropyltrimethoxysilane (APTMS) in order to obtain free reactive -NH<sub>2</sub> groups. 4-(Hydroxymethyl)benzoic acid (HMBA) a linker commonly used in SPPS, was used as the linker. The intermediate and final materials were characterized by FT-IR spectrometry.

The **Fe<sub>3</sub>O<sub>4</sub>-PABA-SiO<sub>2</sub>-SiL-OH** magnetic nanostructured system, newly synthesized for use as a solid support in peptide synthesis was obtained by grafting on the surface of **Fe<sub>3</sub>O<sub>4</sub>-PABA-SiO<sub>2</sub>-1** nanoparticles of a new organic linker system **SiL-OH** with free -CH<sub>2</sub>-OH group, similar to HMBA, obtained from 1,4-dimethylolbenzene and *gamma*-isocyanatopropyltriethoxysilane. The structure of the new linker system **SiL-OH** synthesized was confirmed by <sup>1</sup>H NMR, <sup>13</sup>C NMR and FT-IR and the structure of the new magnetic nanostructured system **Fe<sub>3</sub>O<sub>4</sub>-PABA-SiO<sub>2</sub>-SiL-OH** was confirmed by FT-IR.

The new magnetic nanostructured system **Fe<sub>3</sub>O<sub>4</sub>-PABA-SiO<sub>2</sub>-SiL-OHmw** synthesized for use as a solid support in SPPS was obtained by sequential functionalization of **Fe<sub>3</sub>O<sub>4</sub>-PABA-SiO<sub>2</sub>-2** nanoparticles, with *gamma*-isocyanatopropyltriethoxysilane and 1,4-

dimethylolbenzene using the microwave irradiation in the presence of dibutyltin dilaurate. The structure of the new magnetic nanostructured system **Fe<sub>3</sub>O<sub>4</sub>-PABA-SiO<sub>2</sub>-SiL-OHmw** was confirmed by FT-IR.

The new synthesized nanostructured systems were tested by successfully coupling three different Fmoc-protected amino acids. The different morphologies of the silica secondary shell influence the dispersibility of nanostructured systems in solvents used in solid phase synthesis, but do not affect the performance of the presented peptide synthesis.

The experimental results obtained by FT-MS show the successful obtaining of the proposed peptide sequences (**Lys-Ala-Gly**, **Val-Ile-Lys**, **Gly-Ala-Phe**, **Leu-Ile-Val**); as well as the feasibility of the peptide synthesis method using as a solid support a magnetic nanostructured system through the Fmoc synthesis strategy.

The electrical properties of nanofilms **Fe<sub>3</sub>O<sub>4</sub>-PABA** and **Fe<sub>3</sub>O<sub>4</sub>-PABA-SiO<sub>2</sub> doped with DPPH radical** obtained by the Dip-Coating method was investigated.

The „p” type semiconductor character of the **Fe<sub>3</sub>O<sub>4</sub>-PABA** nanofilm was demonstrated by electrical measurements. The **Fe<sub>3</sub>O<sub>4</sub>-PABA** nanofilm of the „p” type entered the depletion regime with lower leakage current at a positive voltage on the gate. Thin films of different thicknesses (200, 400 and 600 nm) were deposited by the Dip Coating method. Electrical measurements of the **Fe<sub>3</sub>O<sub>4</sub>-PABA** nanofilm demonstrated that the fabricated OTFT (thin film organic transistor) model has a „p” type behavior.

The „n” type character of the **Fe<sub>3</sub>O<sub>4</sub>-PABA-SiO<sub>2</sub> nanofilm doped with DPPH radical** was proved by static measurements. The **Fe<sub>3</sub>O<sub>4</sub>-PABA-SiO<sub>2</sub> nanofilm doped with DPPH radical** was obtained by the Dip Coating method. The homogeneity of the film deposition was highlighted by the homogeneity of the spectral response using the following characterization techniques: MALDI and FT-IR microscopy. The **Fe<sub>3</sub>O<sub>4</sub>-PABA-SiO<sub>2</sub>-4** nanofilm it was also used as a matrix in MALDI analysis. The recorded electrical measurements showed a transistor behavior (TFT type - thin film transistor) with „n” type film.



## ANNEX 2 (Chapter 7) - Identification of peptide fragments

### 2. Identification in the MS spectra of VIK peptide fragments

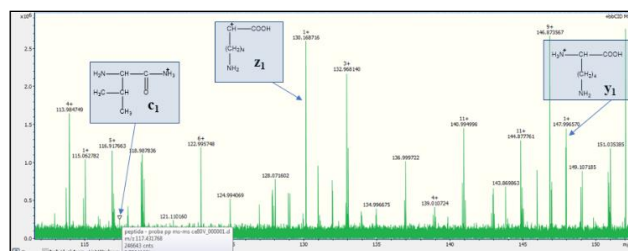


Figure A2.7. Identification in the MS spectrum of **c<sub>1</sub>**, **y<sub>1</sub>**, **z<sub>1</sub>** fragments with m/z 117.43, 130.16, respectively 147.99

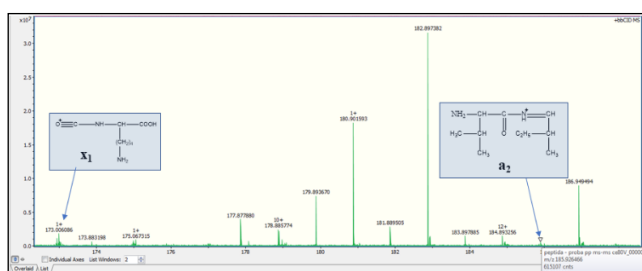


Figure A2.8. Identification in the MS spectrum of **x<sub>1</sub>** and **a<sub>2</sub>** with m/z 173.00, respectively 185.92

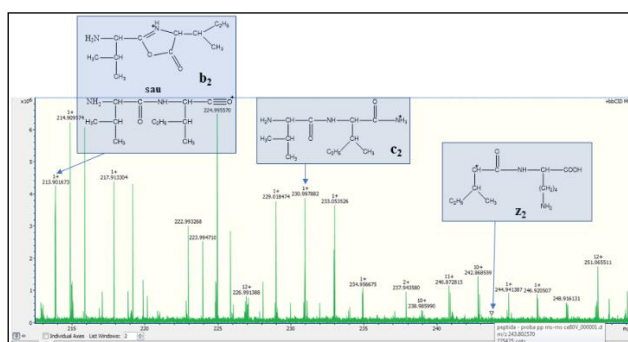


Figure A2.9. Identification in the MS spectrum of **b<sub>2</sub>**, **c<sub>2</sub>** and **z<sub>2</sub>** with m/z 213.90, 230.99, respectively 243.80

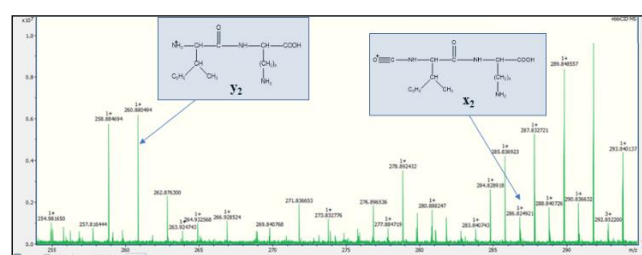


Figure A2.10. Identification in the MS spectrum of **x<sub>2</sub>** and **y<sub>2</sub>** with m/z 286.82 and 260.88

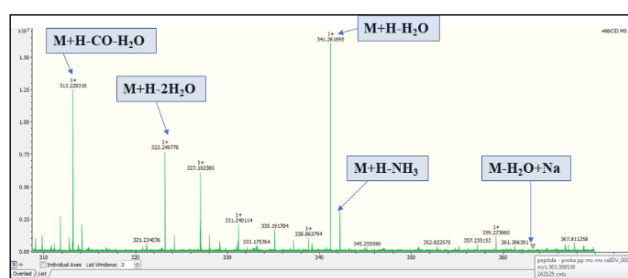


Figure A2.11. Identification in the MS spectrum of **[M+H-H<sub>2</sub>O]<sup>+</sup>**, **[M+H-CO-H<sub>2</sub>O]<sup>+</sup>**, **[M+H-NH<sub>3</sub>]<sup>+</sup>**, **[M-H<sub>2</sub>O+Na]<sup>+</sup>**, **[M+H-2H<sub>2</sub>O]<sup>+</sup>** with m/z 341.26, 313.22, 342.26, 363.30, respectively 323.24

## SELECTIVE BIBLIOGRAPHY

- [26] C. Stutz, I. Bilecka, A.F. Thünemann, M. Niederberger, H.G. Börner, Superparamagnetic core–shell nanoparticles as solid supports for peptide synthesis, *Chemical Communications*, 48 (2012) 7176–7178.
- [59] G.G. Nedelcu, A. Nastro, L. Filippelli, M. Cazacu, M. Iacob, C.O. Rossi, A. Popa, D. Toloman, M. Dobromir, F. Iacomi, Structural characterization of copolymer embedded magnetic nanoparticles, *Applied Surface Science*, 352 (2015) 109–116.
- [62] K. Tadyszak, A. Kertmen, E. Coy, R. Andruszkiewicz, S. Milewski, I. Kardava, B. Scheibe, S. Jurga, K. Chybczynska, Spectroscopic and magnetic studies of highly dispersible superparamagnetic silica coated magnetite nanoparticles, *Journal of Magnetism and Magnetic Materials*, 433 (2017) 254–261.
- [65] M. Abbas, P.B. Rao, M.N. Islam, S.M. Naga, M. Takahashi, C. Kim, Highly stable- silica encapsulating magnetite nanoparticles (Fe<sub>3</sub>O<sub>4</sub>/SiO<sub>2</sub>) synthesized using single surfactantless polyol process, *Ceramics International*, 40 (2014) 1379–1385.
- [78] G. Krylova, M.I. Bodnarchuk, U.I. Tromsdorf, E.V. Shevchenko, D.V. Talapin, H. Weller, Synthesis, Properties and Applications of Magnetic Nanoparticles, in: G. Schmid (Ed.) *Nanoparticles From Theory to Application*, Wiley-VCH, Weinheim, 2010, pp. 239–297.
- [107] R.K. Singh, T.-H. Kim, K.D. Patel, J.C. Knowles, H.-W. Kim, Biocompatible magnetite nanoparticles with varying silica-coating layer for use in biomedicine: physicochemical and magnetic properties, and cellular compatibility, *Journal of Biomedical Materials Research A*, 100 (2012) 1734–1742.
- [136] A. Moroşan, D.E. Mihaiescu, D. Istrati, G. Voicu, A. Fudulu, R. Stan, Polar shell magnetic nanostructured systems for heterogeneous nanophase reactions, *UPB Scientific Bulletin, Series B*, 80 (2018) 53–64.
- [137] C. Ravariu, D.E. Mihaiescu, A. Moroşan, D. Istrati, B. Purcăreanu, R. Cristescu, R. Truşcă, B.Ş. Vasile, Solution for green organic thin film transistors: Fe<sub>3</sub>O<sub>4</sub> nano-core with PABA external shell as p-type film, *Journal of Materials Science: Materials in Electronics*, (2020) 1–11.
- [138] A. Moroşan, D.E. Mihaiescu, D. Istrati, G. Voicu, M. Radu, A. Hanganu, R. Stan, Functionalized silica shell magnetic nanoparticles for nanophase peptide synthesis applications, *Microporous and Mesoporous Materials*, 286 (2019) 45–56.
- [141] P. Launer, Infrared Analysis of Organosilicon Compounds in: B. Arkles, G.L. Larson (Eds.) *Silicon Compounds: Silanes and Silicones*, Gelest, Inc., Morrisville, 2013, pp. 177–180.
- [150] L. Guerrini, R.A. Alvarez-Puebla, N. Pazos-Perez, Surface Modifications of Nanoparticles for Stability in Biological Fluids *Materials*, 11 (2018) 1–28.
- [151] D. Mishra, R. Arora, S. Lahiri, S.S. Amritphale, N. Chandra, Synthesis and Characterization of Iron Oxide Nanoparticles by Solvothermal Method, *Protection of Metals and Physical Chemistry of Surfaces*, 50 (2014) 628–631.
- [167] H. Chen, C. Deng, X. Zhang, Synthesis of Fe<sub>3</sub>O<sub>4</sub>@SiO<sub>2</sub>@PMMA Core–Shell–Shell Magnetic Microspheres for Highly Efficient Enrichment of Peptides and Proteins for MALDI ToF MS Analysis, *Angewandte Chemie International Edition*, 49 (2010) 607–611.
- [170] R. Roto, Surface Modification of Fe<sub>3</sub>O<sub>4</sub> as Magnetic Adsorbents for Recovery of Precious Metals, in: M.A. Chowdhury (Ed.) *Advanced Surface Engineering Research*, IntechOpen, London, 2018, pp. 128–139.
- [173] E. Petrovský, V. Kropáček, M.J. Dekkers, C. deBoer, V. Hoffmann, A. Ambatiello, Transformation of hematite to maghemite as observed by changes in magnetic parameters: Effects of mechanical activation?, *Geophysical Research Letters*, 23 (1996) 1477–1480.
- [181] V.K. Singh, B. Mazhari, Accurate characterization of organic thin film transistors in the presence of gate leakage current, *AIP Advances*, 1 (2011) 042123–042121–042111.
- [186] H. Yang, R. Su, J.S. Wishnok, N. Liu, C. Chen, S. Liu, S.R. Tannenbaum, Magnetic silica nanoparticles for use in matrix-assisted laser desorption ionization mass spectrometry of labile biomolecules such as oligosaccharides, amino acids, peptides and nucleosides, *Microchimica Acta*, 186 (2019) 1–8.
- [193] G. Zhang, R.S. Annan, S.A. Carr, T.A. Neubert, Overview of Peptide and Protein Analysis by Mass Spectrometry, *Current Protocols in Protein Science*, 62 (2010) 16.11.11–16.11.30.
- [194] K.F. Faull, A.N. Dooley, F. Halgand, L.D. Shoemaker, A.J. Norris, C.M. Ryan, A. Laganowsky, J.V. Johnson, J.E. Katz, An Introduction to the Basic Principles and Concepts of Mass Spectrometry-Protein Mass Spectrometry, in: J.P. Whitelegge (Ed.) *Comprehensive Analytical Chemistry*, Elsevier Science, Amsterdam, 2008, pp. 1–40.
- [197] C. Afonso, R.B. Cole, J.-C. Tabet, Dissociation of Even-Electron Ions, in: R.B. Cole (Ed.) *Electrospray and MALDI Mass Spectrometry Fundamentals, Instrumentation, Practicalities, and Biological Applications*, John Wiley & Sons, Inc., New Jersey, 2010, pp. 632–659.
- [199] D.P. Demarque, A.E.M. Crotti, R. Vessecchi, J.L.C. Lopes, N.P. Lopes, Fragmentation reactions using electrospray ionization mass spectrometry: an important tool for the structural elucidation and characterization of synthetic and natural products, *Natural Product Reports*, 33 (2016) 432–455.

## DISSEMINATION OF RESULTS

1. A. Moroşan, D. E. Mihaiescu, D. Istrati, G. Voicu, A. Fudulu, R. Stan, Polar shell magnetic nanostructured systems for heterogeneous nanophase reactions, **U.P.B. Sci. Bull. Ser B**, 2018, 80 (3) 53-64, ISSN 1454-2331
2. A. Moroşan, D. E. Mihaiescu, D. Istrati, G. Voicu, M. Radu, A. Hanganu, R. Stan, Functionalized silica shell magnetic nanoparticles for nanophase peptide synthesis applications, **Microporous and Mesoporous Materials**, 2019, 286, 45–56. DOI: 10.1016/j.micromeso.2019.05.018 (IF= 4.551)
3. C. Ravariu, D. E. Mihaiescu, A. Moroşan, D. Istrati, B. Purcăreanu, R. Cristescu, R. Truşcă, B. Ş. Vasile, „Solution for green organic thin film transistors: Fe<sub>3</sub>O<sub>4</sub> nano-core with PABA external shell as p-type film”, **Journal of Materials Science: Materials in Electronics**, 2020, 1-11. (IF= 2.220)

## INTERNATIONAL CONFERENCES

### *Oral presentations*

1. A. Moroşan, D. Istrati, D. E. Mihaiescu, ***Peptide synthesis on magnetic nanostructured support using Fmoc strategy***, Seminar: "ACS on Campus", Universitatea POLITEHNICA din Bucureşti, 13.05.2016, Bucureşti, Romania
2. A. Moroşan, R. Stan, D. Istrati, D. E. Mihaiescu, ***Alternative hybrid nanostructured support for solid phase peptide synthesis***, 20th Romanian International Conference on Chemistry and Chemical Engineering, September 6-9, 2017, Poiana Brasov, Romania

### *Posters*

3. A. Moroşan, D. Istrati, D. E. Mihaiescu, A. Fudulu, A. Marton, R. Stan, ***Synthese des peptides sur support magnetique nanostructure à l'aide de la strategie Fmoc***, 9<sup>ème</sup> Colloque Franco-Roumain de Chimie Appliquée (COFrRoCA), 29 Juin-1 Juillet 2016, Clermont Ferrand, France
4. A. Moroşan, D. Istrati, R.L.Stan, B. Trică, G. Vasilievici, D.E. Mihaiescu, ***Functionalized silica shell magnetic nanoparticles for nanophase peptide synthesis applications***, 15th ICNN – NN18-NANOTECHNOLOGY 2018, 2-7.07.2018, Thessaloniki, Greece
5. A. Moroşan, D. E. Mihaiescu, D. Istrati, R. Stan, G. Voicu, B. Vasile, ***New approaches of peptides synthesis***, 9th ICOSECS 2019, 8-11.05.2019, Targoviste, Romania
6. A. Moroşan, D. Istrati, D. E. Mihaiescu, C. Ravariu, B. Vasile, ***Nanocomposites Based on SET – Active Organic Compounds for Electron Transfer Applications in Electronics***, 31<sup>st</sup> International Conference and Expo on Nanosciences and Nanotechnology, 18-19.11.2019, Paris, France (moderator)

### *Awards*

- Prix au meilleur poster:** „*Synthese des peptides sur support magnetique nanostructure à l'aide de la strategie Fmoc*”, 9<sup>ème</sup> Colloque Franco-Roumain de Chimie Appliquée (COFrRoCA), 29 Juin-1 Juillet 2016, Clermont Ferrand, France